ORNL/TM-12388

Computer Science and Mathematics Division

Mathematical Sciences Section

ARE BILINEAR QUADRILATERALS BETTER THAN LINEAR TRIANGLES?

E. F. D'Azevedo

Computer Science and Mathematics Division
Oak Ridge National Laboratory
P.O. Box 2008, Bldg. 6012
Oak Ridge, TN 37831-6367

Date Published: August 1993

Research supported by the Applied Mathematical Sciences subprogram of the Office of Energy Research, U.S. Department of Energy and in part by the Information Technology Research Centre, which is funded by the Province of Ontario.

Prepared by the
Oak Ridge National Laboratory
Oak Ridge, Tennessee 37831
managed by
Lockheed Martin Energy Research Corp.
for the
U.S. DEPARTMENT OF ENERGY
under Contract No. DE-AC05-84OR21400

Contents

List of Tables

List of Figures

ARE BILINEAR QUADRILATERALS BETTER THAN LINEAR TRIANGLES?

E. F. D'Azevedo

Abstract

This paper compares the theoretical effectiveness of bilinear approximation over quadrilaterals with linear approximation over triangles. Anisotropic mesh transformation is used to generate asymptotically optimally efficient meshes for piecewise linear interpolation over triangles and bilinear interpolation over quadrilaterals. For approximating a convex function, although bilinear quadrilaterals are more efficient, linear triangles are more accurate and may be preferred in finite element computations; whereas for saddle-shaped functions, quadrilaterals may offer a higher order approximation on a well-designed mesh. A surprising finding is different grid orientations may yield an order of magnitude improvement in approximation accuracy.

1. Introduction

This paper compares the theoretical effectiveness of bilinear approximation over quadrilaterals with linear approximation over triangles. The novelty is in the use of anisotropic mesh transformation to generate asymptotically optimally efficient meshes in the comparison. Elementary analysis based on a simple quadratic data model is used. Although both linear and bilinear interpolants are $O(h^2)$ accurate, the results suggest linear triangles are *always* more accurate than general convex bilinear quadrilaterals in approximating a convex function but bilinear approximation may offer a higher order approximation for saddle-shaped functions on a well-designed mesh. A surprising finding is different grid orientations may yield an order of magnitude "super-convergence" improvement in approximation accuracy. This work is a basic study on optimal meshes with the intention of gaining insight into the more complex meshing problems in finite element analysis.

We consider the problem of interpolating a given smooth data function with continuous piecewise linear triangles or bilinear quadrilaterals over a domain to satisfy a given error tolerance. A mesh that achieves this error tolerance with the *fewest* elements is defined to be optimally efficient. Intuitively, one would expect smaller and denser elements in regions where the function has sharp peaks or large variations. Since each convex quadrilateral can be split across either one of the diagonals into two triangles, one can imagine embedding a refined triangular mesh within the quadrilateral mesh. A practical question arises as to whether the bilinear approximation over quadrilaterals or linear approximation over triangles is more effective.

To make a fair comparison, we need to compare bilinear approximation over an "optimal" quadrilateral mesh versus linear approximation over an "optimal" triangular mesh. Provably optimal triangular meshes [2, 4] have been produced by anisotropic mesh transformation.

Anisotropic mesh transformation is emerging as an effective technique for unstructured grid generation where the vertex distribution is highly non-uniform. The central idea is to control the element shapes and sizes by specifying a symmetric metric tensor that measures the approximation error. The metric tensor determines the corresponding anisotropic transformation. The anisotropic mesh is then the image of a uniform mesh of optimal shape elements under the anisotropic transformation. Simpson [9] gives a survey on anisotropic meshes.

Nadler [7], D'Azevedo and Simpson [3, 4], and D'Azevedo [2] have studied *local* anisotropic transformation for the generating of optimally efficient triangular meshes. Peraire et al. [8] applied anisotropic transformation in mesh generation for dynamic remeshing in solving compressible flow problems. In these works, piecewise linear approximation of a quadratic function is used as the model for local analysis. In this paper we extend a similar analysis to bilinear approximation on quadrilateral patches.

An outline of the paper follows. In §2, we review the key ideas in [2] for generating optimally efficient triangular meshes. In §3, we consider error properties of bilinear interpolation. We consider the optimal geometry for quadrilateral patches in §4. We compare the effectiveness of quadrilaterals versus triangular meshes using the local quadratic model in §5. Numerical experiments and the results are described in §7. Finally §8 gives a brief summary.

2. Triangular Patch

This section is a brief review of the basic ideas in [2] for determining optimal triangle geometry. We show a linear transformation of a regular mesh of optimal-shape triangles yields an optimally efficient mesh for interpolating a quadratic function.

2.1. Quadratic Model

We shall consider a local analysis where we assume the data function $f(x, y)$ in the neighborhood of (x_c, y_c) is well approximated by its quadratic Taylor expansion,

$$\begin{aligned} f(x,y) &= f(x_c+dx, y_c+dy) \\ &\approx f(x_c,y_c) + \nabla f(x_c,y_c)[dx,dy] + \frac{1}{2}[dx,dy]H[dx,dy]^t . \end{aligned} \tag{1}$$

Let the error formula be $E_T(x, y) = p_\ell(x, y) - f(x, y)$, where $p_\ell(x, y)$ is the linear interpolant. By our assumption, $E_T(x, y)$ is a quadratic function and level curves for $E_T(x, y) = c$ form a family of conics with a common center at (x_c, y_c). They form a family of ellipses if $\det(H) > 0$, and hyperbolas if $\det(H) < 0$. Note by the interpolation condition, the curve $E_T(x, y) = 0$ passes through all vertices of the triangle. If $\det(H) > 0$ (conic is an ellipse) then $E_T(x, y)$ attains the local maximum at the center (x_c, y_c); otherwise, $\det(H) < 0$ (conic is a hyperbola) the maximum error is attained at the midpoint of an edge. The error at a displacement from the center is given by

$$E_T(x_c+dx, y_c+dy) = E_T - \frac{1}{2}[dx,dy]H[dx,dy]^t, \quad E_T = E_T(x_c,y_c) . \tag{2}$$

The key insight in [2] is in interpreting the Hessian matrix H in (2) as a symmetric metric tensor. Let the symmetric Hessian matrix be diagonalizable as

$$\begin{aligned} H &= Q^t \begin{bmatrix} \lambda_1 & 0 \\ 0 & \lambda_2 \end{bmatrix} Q = S^t \begin{bmatrix} 1 & 0 \\ 0 & \epsilon \end{bmatrix} S, \quad \text{where } \epsilon = \text{sign}(\det(H)), \\ S &= \begin{bmatrix} \sqrt{|\lambda_1|} & 0 \\ 0 & \sqrt{|\lambda_2|} \end{bmatrix} Q, \quad \text{and } Q \text{ is orthogonal, } Q^tQ = I . \end{aligned} \tag{3}$$

Note that transformation S is essentially a rotation to align eigenvectors along the coordinate axes then followed by a simple scaling. Under this transformation S, the expression $[dx, dy]H[dx, dy]^t$ reduces to $(d\tilde{x})^2 + \epsilon(d\tilde{y})^2$, where $[\tilde{x}, \tilde{y}]^t = S[x, y]^t$. The error function can be rewritten as

$$\begin{aligned} E_T(x_c + dx, y_c + dy) &= E_T - \frac{1}{2}[dx, dy]H[dx, dy]^t \\ &= E_T - \frac{1}{2}\left((d\tilde{x})^2 + \epsilon(d\tilde{y})^2\right) \\ &= \tilde{E}_T(\tilde{x}_c + d\tilde{x}, \tilde{y}_c + d\tilde{y}), \end{aligned} \tag{4}$$

where $\tilde{E}_T(\tilde{x}, \tilde{y})$ denotes the corresponding error function under transformation S in $(\tilde{x}, \tilde{y})$-space. The error expression $\tilde{E}_T(\tilde{x}, \tilde{y})$ has no preferred direction (except for the sign), hence we shall call the $(\tilde{x}, \tilde{y})$-space the "isotropic" space.

2.2. Optimal shape

In the following, we shall determined the best triangle shape that minimizes the interpolation error. We can determine the "efficiency" of the elements by computing their ratio of Error to Area. A small ratio indicates a more efficient element, i.e. one can achieve a lower error tolerance and tile the domain with about the same number of elements.

We consider first the case $f(x, y)$ is convex ($\det(H) > 0, \epsilon = 1$) and level curves or contours of $\tilde{E}_T(\tilde{x}, \tilde{y})$ are concentric circles given by

$$\tilde{E}_T(\tilde{x}_c + d\tilde{x}, \tilde{y}_c + d\tilde{y}) = E_T - \frac{1}{2}\left((d\tilde{x})^2 + (d\tilde{y})^2\right) \ . \tag{5}$$

Let $\tilde{T}$ be the transformed image of triangle T over the isotropic space, with vertices at $(\tilde{x}_1, \tilde{y}_1)$, $(\tilde{x}_2, \tilde{y}_2)$ and $(\tilde{x}_3, \tilde{y}_3)$. The circum-circle of $\tilde{T}$ corresponds to the level curve of value zero. Hence the radius of this circum-circle is sqrt($2|E_T|$) and relates directly to the maximum error attainable (at the center). If this center is exterior to triangle T, the maximum error is attained at the mid-point of the longest edge (of length L) with value $L^2/8$. We can easily see that an equilateral triangle covers the most area for a fixed circum-circle; therefore an equilateral triangle for $\tilde{T}$ is of optimal-shape.

If $f(x, y)$ is not convex but has a saddle-shaped graph ($\det(H) < 0$, $\epsilon = -1$), then

$$\begin{aligned} \tilde{E}_T(\tilde{x}, \tilde{y}) &= \tilde{E}_T(\tilde{x}_c + d\tilde{x}, \tilde{y}_c + d\tilde{y}) \\ &= E_T - \frac{1}{2}\left((d\tilde{x})^2 - (d\tilde{y})^2\right) \\ &= E_T - \frac{1}{2}\left((\tilde{x} - \tilde{x}_c)^2 - (\tilde{y} - \tilde{y}_c)^2\right) \ . \end{aligned} \tag{6}$$

We note that the error function $\tilde{E}_T(\tilde{x}, \tilde{y})$ is a harmonic function and thus attains its extrema on the boundary of $\tilde{T}$. By calculus, we can show that the local extrema along edge $(\tilde{x}_i, \tilde{y}_i)$, $(\tilde{x}_j, \tilde{y}_j)$ is attained at the midpoint with value

$$\tilde{E}\left(\frac{\tilde{x}_i + \tilde{x}_j}{2}, \frac{\tilde{y}_i + \tilde{y}_j}{2}\right) \quad = \quad \frac{1}{8}\left|(\tilde{x}_i - \tilde{x}_j)^2 - (\tilde{y}_i - \tilde{y}_j)^2\right| \ .$$

The details for finding the optimal-shape triangle in this case are found in [2]. The optimal-shape triangle geometry that minimizes the efficiency ratio (Error / Area) is not unique, but the same maximum error is attained at the mid-point of each edge.

From the above two results on optimal-shape triangles, we see that a *regular* mesh of optimal-shape triangles over the isotropic $(\tilde{x}, \tilde{y})$-space corresponds to an optimally efficient mesh over the original (x, y)-space. Every triangle attains the same maximum error; moreover, these triangles cover the most area for the error attained and so are optimally efficient. Since the linear transformation S is basically a rotation followed by a rescaling of coordinate axes, we find the areas of triangles are scaled accordingly. Hence the inverse transformation S^{-1}, maps this regular mesh to produce an optimally efficient mesh in the original (x, y)-space.

2.3. Differential Geometry

The *constant* Hessian Matrix H in (1) determines the coordinate transformation S that maps $[\tilde{x}, \tilde{y}]^t = S[x, y]^t$ so that

$$[dx, dy]H[dx, dy]^t = (d\tilde{x}^2 + \epsilon d\tilde{y}^2) \ .$$

For more general functions, we may view the Hessian matrix $H(x, y)$ as a metric tensor for measuring the interpolation error $[dx, dy]H[dx, dy]^t$. Thus we need to determine $(\tilde{x}(x, y), \tilde{y}(x, y))$, a *continuous* transformation that satisfies $[dx, dy]H[dx, dy]^t = d\tilde{x}^2 + \epsilon d\tilde{y}^2$. The conditions for finding the anisotropic coordinate transformation $(\tilde{x}(x, y), \tilde{y}(x, y))$ are given by a classical result in differential geometry for characterizing a "flat" space [11]: that the Riemann-Christoffel tensor formed from the metric tensor H is identically zero. In this case, a sufficient condition is for $H = \{h_{ij}\}$ to satisfy

$$K_1 h_{11} + K_2 h_{12} + K_3 h_{22} = 0$$

for some constants K_1, K_2, K_3. The coordinate transformation $(\tilde{x}(x, y), \tilde{y}(x, y))$ may be found by solving an initial value ordinary differential equation. Again, the inverse transformation $(x(\tilde{x}, \tilde{y}), y(\tilde{x}, \tilde{y}))$ maps a regular mesh of optimal shaped triangles to yield an optimally efficient mesh.

3. Quadrilateral Patch

In this section, we derive the error term for bilinear approximation of a quadratic data function.

We shall use the isoparametric formulation (commonly used in finite element analysis) by considering basis functions over the normalized (p, q)-space over the unit square, $0 \leq p, q \leq 1$. Basis functions are

$$\begin{aligned} \phi_1(p,q) &= (1-p)(1-q), & \phi_2(p,q) &= p(1-q), \\ \phi_3(p,q) &= pq, & \phi_4(p,q) &= (1-p)q\ , \end{aligned} \tag{7}$$

that satisfy $\phi_i(x_j, y_j) = \delta_{ij}$, and sum to one, $1 = \sum_{i=1}^{i=4} \phi_i(p,q)$.

Mapping from (p, q) to the original (x, y)-space is by

$$\begin{aligned} x(p,q) &= x_1\phi_1(p,q) + x_2\phi_2(p,q) + x_3\phi_3(p,q) + x_4\phi_4(p,q) \\ y(p,q) &= y_1\phi_1(p,q) + y_2\phi_2(p,q) + y_3\phi_3(p,q) + y_4\phi_4(p,q) \end{aligned} \tag{8}$$

that maps vertex $(0,0)$ to (x_1, y_1), vertex $(1,0)$ to (x_2, y_2), $(1,1)$ to (x_3, y_3) and $(0,1)$ to (x_4, y_4). The bilinear interpolant (over (p, q)-space) is given by

$$p_b(x(p,q), y(p,q)) = \sum_{i=1}^{i=4} f(x_i, y_i)\phi_i(p,q)\ . \tag{9}$$

4. Optimal Shape

In the following, we shall determine the best quadrilateral shape that minimizes the interpolation error. The error function for quadratic interpolation over a *parallelogram* can be shown by direct algebraic expansion (see Appendix A) to be

$$\begin{aligned} E_Q(p,q) &= p_b(x(p,q), y(p,q)) - f(x(p,q), y(p,q)) \\ &= E_Q - \frac{1}{2}\left(\mu_1(p-p_c)^2 + \mu_2(q-q_c)^2\right)\ , \end{aligned} \tag{10}$$

with centroid at $[p_c, q_c] = [1/2, 1/2]$,

$$[u_x, u_y] = [x_2 - x_1, y_2 - y_1], \quad [v_x, v_y] = [x_4 - x_1, y_4 - y_1],$$

$$\begin{aligned} E_Q &= E_Q(p_c, q_c) = \frac{1}{8}(\mu_1 + \mu_2)\ , \\ 0 &= \frac{\partial}{\partial p}E_Q(p_c, q_c) = \frac{\partial}{\partial q}E_Q(p_c, q_c)\ , \end{aligned} \tag{11}$$

$$\mu_1 \;=\; [u_x, u_y]H[u_x, u_y]^t, \quad \mu_2 = [v_x, v_y]H[v_x, v_y]^t \,.$$

For a convex function ($\det(H) > 0$), μ_1 and μ_2 are positive, hence the maximum error is attained at the centroid $[p_c, q_c]$.

For this convex case, we can show a square over the isotropic space is of optimal shape by minimizing the efficiency ratio (Error / Area). Since the isoparametric bilinear interpolant (9) exactly fits linear functions [5], the error attained at the centroid (x_c, y_c) (which is a lower bound on the maximum error) can be written as

$$\begin{aligned} E_M &= \frac{1}{4}\left(\sum_{i=1}^{i=4} \tfrac{1}{2}[x_i, y_i]H[x_i, y_i]^t\right) - \tfrac{1}{2}[x_c, y_c]H[x_c, y_c]^t \qquad (12)\\ &= \frac{1}{8}\left(\sum_{i=1}^{i=4} \left([x_i, y_i]H[x_i, y_i]^t - [x_c, y_c]H[x_c, y_c]^t\right)\right)\\ [x_c, y_c] &= [(x_1 + x_2 + x_3 + x_4)/4, (y_1 + y_2 + y_3 + y_4)/4] \,. \qquad (13) \end{aligned}$$

This expression can be further simplified over the isotropic space where H is the identity,

$$\begin{aligned} E_M &= \frac{1}{8}\left(\sum_{i=1}^{i=4} \left((\tilde{x}_i^2 + \tilde{y}_i^2) - (\tilde{x}_c^2 + \tilde{y}_c^2)\right)\right)\\ &= \frac{1}{8}\left((\tilde{x}_1^2 + \tilde{x}_2^2 + \tilde{x}_3^2 + \tilde{x}_4^2) - 4\tilde{x}_c^2 + (\tilde{y}_1^2 + \tilde{y}_2^2 + \tilde{y}_3^2 + \tilde{y}_4^2) - 4\tilde{y}_c^2\right)\\ &= \frac{1}{8}(L_1^2 + L_2^2 + L_3^2 + L_4^2), \quad \text{with } L_i^2 = (\tilde{x}_i - \tilde{x}_c)^2 + (\tilde{y}_i - \tilde{y}_c)^2, \end{aligned}$$

where $[\tilde{x}_i, \tilde{y}_i]^t = S[x_i, y_i]^t$ and $[\tilde{x}_c, \tilde{y}_c]^t = S[x_c, y_c]^t$ are the corresponding coordinates over the isotropic space. The area of this transformed convex quadrilateral is (see Figure 1)

$$\text{Area} \;=\; \tfrac{1}{2}\left(L_1 L_2 \sin(\theta_1) + L_2 L_3 \sin(\theta_2) + L_3 L_4 \sin(\theta_3) - L_4 L_1 \sin(\theta_1 + \theta_2 + \theta_3)\right).$$

Since the isotropic transformation S in (3) is a rotation followed by a rescaling of coordinate axis, the area of quadrilateral over the isotropic space is scaled by $\text{sqrt}(|\lambda_1\lambda_2|) = \text{sqrt}(\det(H))$ (intrinsic to H). By Calculus, we can show this ratio of E_M / Area is minimized and *attained* by a square with $L_1 = L_2 = L_3 = L_4$ and $\theta_1 = \theta_2 = \theta_3 = \pi/4$. Hence the most efficient shape among *all* general convex bilinear quadrilaterals is a square over the isotropic space with an efficiency ratio of $1/4$.

If $f(x, y)$ is saddle-shaped ($\det(H) < 0$), the error expression for a parallelogram is still

$$E_Q(p, q) \;=\; \frac{1}{8}(\mu_1 + \mu_2) - \frac{1}{2}(\mu_1 (p - p_c)^2 + \mu_2 (q - q_c)^2) \,.$$

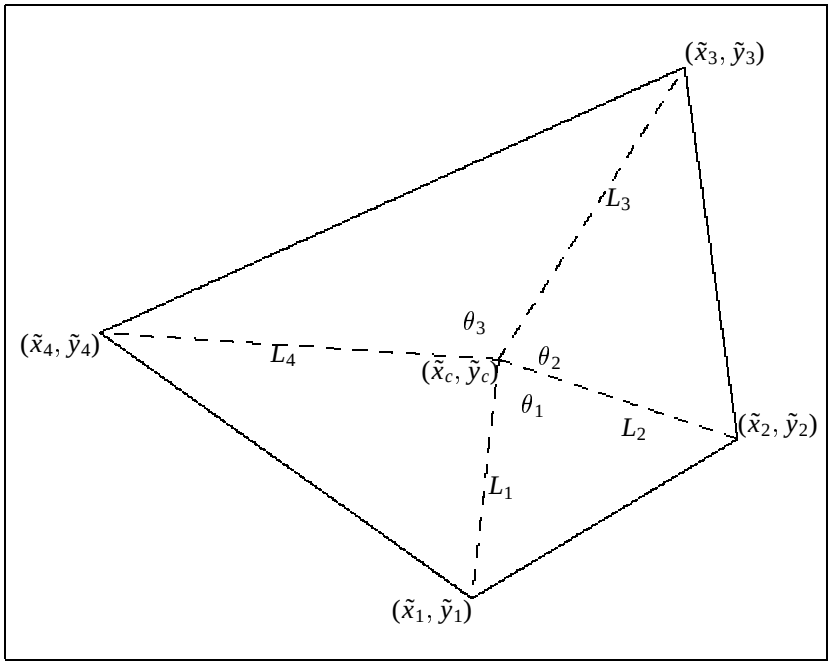

Figure 1: Convex quadrilateral over isotropic space.

Under the anisotropic transformation S,

$$\mu_1 \;=\; \tilde{u}_x^2 - \tilde{u}_y^2, \quad \mu_2 = \tilde{v}_x^2 - \tilde{v}_y^2 \,, \quad \begin{bmatrix} \tilde{u}_x & \tilde{v}_x \\ \tilde{u}_y & \tilde{v}_y \end{bmatrix} = S \begin{bmatrix} u_x & v_x \\ u_y & v_y \end{bmatrix} \,.$$

Now both μ_1 and μ_2 vanish for

$$[\tilde{u}_x, \tilde{u}_y] \;=\; [L, L], \quad [\tilde{v}_x, \tilde{v}_y] = [-L, L] \quad , \tag{14}$$

which correspond to a square rotated by $\pi/4$. The above indicates an "exact fit" ($E_Q(p,q) = 0$) if $\mu_1 = \mu_2 = 0$. This suggests bilinear approximation is a better interpolant than linear interpolation and the simple quadratic model is inadequate to fully capture the error properties in this case.

To summarize, a square over the isotropic space in any orientation is optimal for the elliptic case, and a square rotated by $\pi/4$ is optimal for the hyperbolic case.

5. Comparison of quadrilaterals versus triangles

In this section, we shall show a refined triangulation produced by the Delauney Triangulation (DT) will always produce better accuracy for approximating a *convex* quadratic function. We shall apply the geometric interpretation of the maximum interpolation error over the transformed isotropic space.

Theorem 1. *Any convex quadrilateral over the isotropic space can be decomposed into two triangles with no increase in maximum interpolation error for approximating a convex quadratic.*

Proof. We shall use the Delauney Triangulation (DT) [3] in selecting the diagonal for decomposing the general convex quadrilateral into two triangles. The DT has an interesting properties that three vertices form a triangle in DT iff no other vertex is interior to the circumcircle formed by these vertices. This is also commonly known as the "empty circle" property.

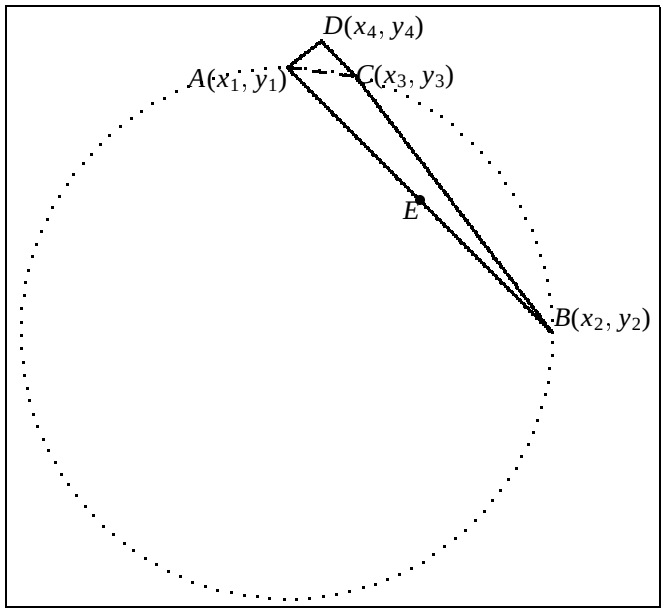

Figure 2: Maximum triangulation error attained on boundary edge.

Case 1. The maximum error of the DT is attained at the mid-point (E) of a boundary edge (see Figure 2). In this case the error attained is due to linear interpolation along the edge AB, with value $|AB|^2/8$. Since the isoparametric bilinear interpolant over the quadrilateral also reduces to linear interpolation along the boundary edge, the maximum error for bilinear quadrilateral cannot be less than this value. Therefore the theorem holds.

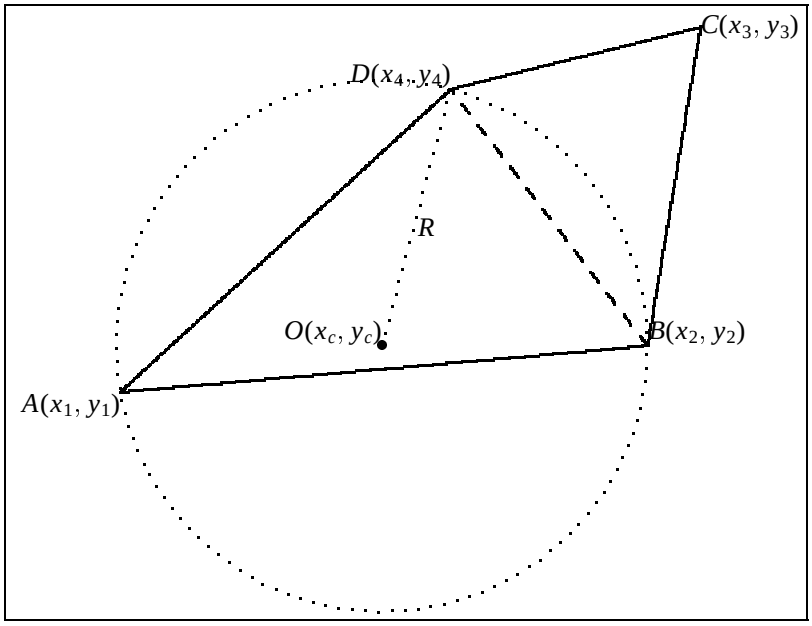

Figure 3: Maximum triangulation error attained at center of circum-circle.

Case 2. The maximum error of the DT is attained at the center of circum-circle, (x_c, y_c) (see Figure 3). For simplicity and without loss of generality, we perform a translation such that the isotropic quadratic data function is $\frac{1}{2}((x - x_c)^2 + (y - y_c)^2)$. The maximum error is $R^2/2$, where R is the radius of the circum-circle. The interpolation error given by the quadrilateral is (9),

$$\begin{aligned} E_Q(x_c, y_c) &= \left(\sum_{i=1}^{i=4} f_i \phi_i(p, q) \right) - f(x_c, y_c), \quad f_i = f(x_i, y_i) \\ &= \left((1 - \phi_3(p, q)) R^2/2 + \phi_3(p, q) f_3 \right) - 0 \end{aligned} \tag{15}$$

since $f_1 = f_2 = f_3 = R^2/2$ and $f(x_c, y_c) = 0$. We have

$$f(x_3, y_3) = ((x_3 - x_c)^2 + (y_3 - y_c)^2)/2 > R^2/2 \,, \tag{16}$$

and therefore the error attained by quadrilateral at (x_c, y_c) is higher than $R^2/2$, thus the theorem holds.

Cases 1 and 2 are exhaustive since the maximum error of the DT cannot be attained at the the mid point of a diagonal, unless it also satisfies Case 1 or Case 2 as in a square (see Figure 4). We have $\angle BCD \leq \pi/2$ to satisfy the "empty circle" property. If $\angle CDB > \pi/2$ (similar argument

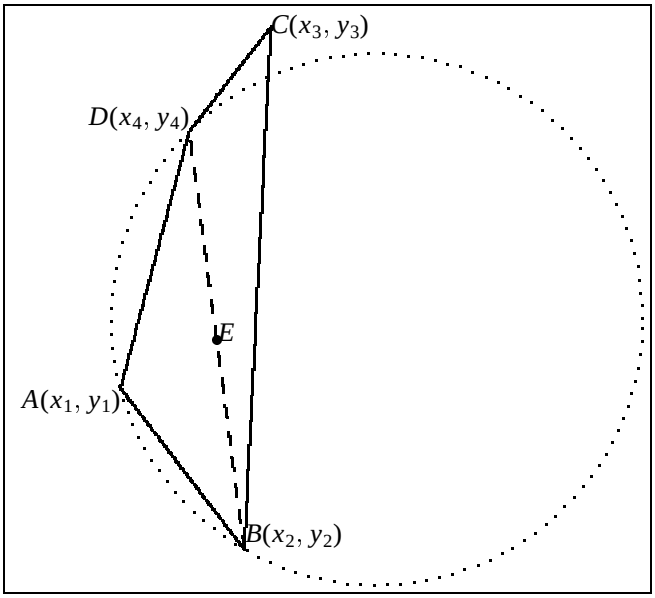

Figure 4: Maximum triangulation error cannot be on diagonal.

for $\angle CBD > \pi/2$), then by Cosine rule for triangles,

$$|BC|^2 = |CD|^2 + |BD|^2 - 2|CD||BD|\cos(\angle CDB) \quad > \quad |BD|^2 \,, \tag{17}$$

thus the maximum error is attained in $\triangle BCD$ on edge BC (Case 1). The remaining alternative is where $\triangle BCD$ forms an acute triangle. Then $\triangle BCD$ will have a larger maximum error given in terms of radius of circum-circle, which is covered in Case 2.

Therefore over the isotropic space, the DT refined linear triangulation is more accurate than the isoparametric bilinear quadrilateral.

This theorem suggests if the data function is not saddle-shaped, the refine DT triangulation (over the isotropic space) produced above will yield better approximation accuracy, even on arbitrary meshes of general convex quadrilaterals.

5.1. Comparison of efficiency ratio

For the optimal shape equilateral triangle, the area, A_T, is $\sqrt{3}L^2/4$, from (4) we obtain an efficiency ratio of

$$\frac{E_T}{A_T} = \frac{L^2/6}{\sqrt{3}L^2/4} = 2\sqrt{3}/9 \approx 0.385 \,.$$

Area of the optimal square configuration is L^2, thus the ratio is $1/4 = 0.25$. Hence for an *element by element* comparison, the quadrilateral is more efficient. In other words, if we were

to approximate a function with either N quadrilaterals or N triangles, quadrilaterals are preferred.

On the other hand, triangles may have advantages over quadrilaterals for finite element computations. Matrix assembly and the solution of the sparse linear equations are commonly the most intensive calculations. If we decompose a quadrilateral mesh into triangles as done above, no extra nodes are introduced. There will be twice as many triangular elements but the resulting assembled matrix has a similar sparsity pattern and the same number of unknowns. Matrix assembly with a *general* convex quadrilateral usually requires costly evaluations of the Jacobian distortion in numerical quadrature over the isoparametric space, whereas assembly of linear triangle elements is simpler. Therefore if computation with N quadrilaterals is as costly as using $2N$ triangles, then triangles are preferred due to their better accuracy and simplicity. The actual computation costs may depend on the implementation of the finite element code.

Consider the approximation of a saddle-shaped function by a square (unrotated) over the isotropic space. The error formula gives

$$\begin{aligned} E_Q(p,q) &= \frac{1}{8}(\mu_1+\mu_2) - \frac{1}{2}(\mu_1(p-p_c)^2 + \mu_2(q-q_c)^2), \quad (p_c,q_c) = (\tfrac{1}{2},\tfrac{1}{2}) \\ &= -\frac{1}{2}((p-p_c)^2L^2 - (q-q_c)^2L^2), \quad \text{where } \mu_1 = L^2 = -\mu_2\,. \end{aligned} \tag{18}$$

The maximum error is attained at the mid-point of each edge. Let $(p,q) = (1,1/2)$, then $E_Q = L^2/8$. This gives an efficiency ratio of $1/8 = 0.125$. One optimal triangle shape for saddle-shaped function is the triangle with vertices at $(0,0)$, $(L,0)$, $(1/2L, \sqrt{5}/2L)$ over the isotropic space [2], which has area $\sqrt{5}L^2/4$. The maximum error is $L^2/8$ and attained at the mid-point of each edge. This gives an efficiency ratio of $1/(2\sqrt{5}) \approx 0.224$. Thus over the isotropic space, a mesh with N (unrotated) squares should yield roughly the same accuracy as $2N$ triangles. This is verified in the numerical experiments.

6. Extensions to three dimensions

The previous results for linear triangles and bilinear quadrilaterals extend to tetrahedrons and hexahedral bricks in three dimensions.

6.1. Error for tetrahedron

To determine the maximum error attained over the tetrahedron in the transformed isotropic space, we have to consider three cases.

Case 1. The center of the circum-sphere $(\tilde{x}_c, \tilde{y}_c, \tilde{z}_c)$ is interior to the tetrahedron and the maximum error, $R^2/2$, is attained at the circum-center where R is the radius of the circum-sphere.

Case 2. The center is exterior and the closest point from the center to the tetrahedron is interior to a face. Let this closest point on this face be $(\tilde{x}_f, \tilde{y}_f, \tilde{z}_f)$, then $(\tilde{x}_f, \tilde{y}_f, \tilde{z}_f)$ is the center of the circum-circle of that face and the maximum error attained is

$$R^2/2 - \frac{1}{2}d^2 = r^2/2,$$

where r is the radius of circum-circle (see Figure 5).

Case 3. The center $(\tilde{x}_c, \tilde{y}_c, \tilde{z}_c)$ is exterior and the closest point to the tetrahedron $(\tilde{x}_m, \tilde{y}_m, \tilde{z}_m)$ is the mid point of an edge. If we consider the great circle on the circum-sphere through the ends of this edge, we have $R^2 = d^2 + (L/2)^2$, where L is the length of this edge. We see the maximum error is attained at this closest point $(\tilde{x}_m, \tilde{y}_m, \tilde{z}_m)$ that is the midpoint of the *longest* edge (see Figure 6). The maximum error attained is

$$R^2/2 - \frac{1}{2}d^2 = L^2/8\,.$$

Note that in all three cases, the maximum error is bounded by $L^2/8$ where L is length of the longest edge. A regular tetrahedron occupies the most volume for a fixed circum-sphere and is the most efficient shape with an efficiency ratio

$$\frac{\text{Error}}{\text{Volume}} = \frac{R^2/2}{8\sqrt{3}R^3/27} \approx 0.9743/R\,. \tag{19}$$

Unfortunately, unlike the equilateral triangle in two dimensions, the regular tetrahedron cannot fill three-dimensional space. The BCC tetrahedron (with vertices at $(0,0,0)$, $(2,0,0)$, $(1,1,1)$, $(-1,1,1)$) is conjectured [6, 10, 12] is to be the best shaped tetrahedron that fills space. Moore [6] shows among a one-parameter family of space filling tetrahedrons, the BCC tetrahedron has the best aspect ratio. Its efficiency ratio is

$$\frac{\text{Error}}{\text{Volume}} = \frac{R^2/2}{16\sqrt{5}R^3/75} \approx 1.048/R\,. \tag{20}$$

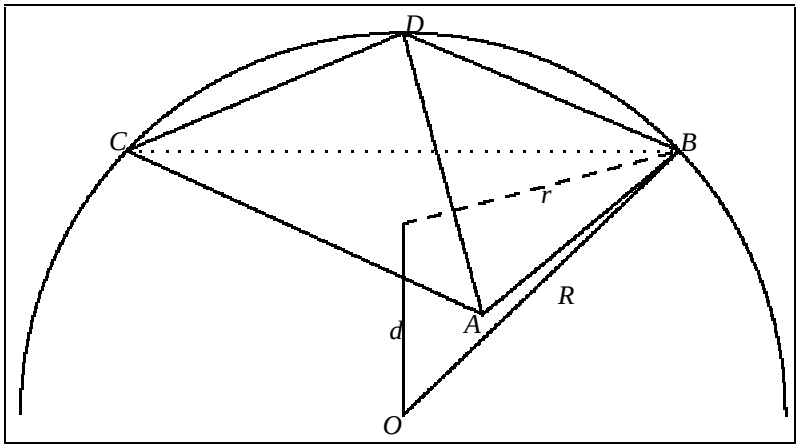

Figure 5: Closest point interior to a face.

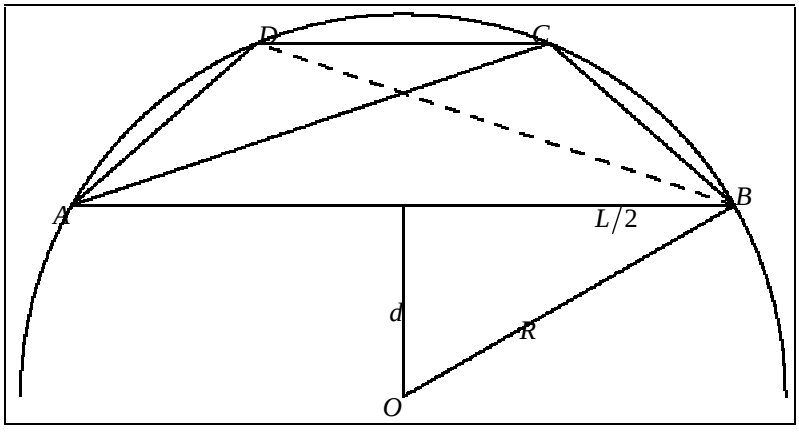

Figure 6: Closest point at midpoint of edge.

6.2. Error for hexahedral brick

Again we consider the isoparametric formulation over the unit cube, $0 \le p, q, r \le 1$,

$$x(p,q,r) = \sum_{i=1}^{i=8} x_i \phi_i(p,q,r), \quad p_\ell(p,q,r) = \sum_{i=1}^{i=8} f_i \phi_i(p,q,r), \quad \text{where} \tag{21}$$

(22)

$$\begin{aligned} \phi_1 = (1-p)(1-q)(1-r), \quad \phi_2 &= p(1-q)(1-r), \\ \phi_3 = pq(1-r), \quad \phi_4 &= (1-p)q(1-r), \\ \phi_5 = (1-p)(1-q)r, \quad \phi_6 &= p(1-q)r, \\ \phi_7 = pqr, \quad \phi_8 &= (1-p)qr\,. \end{aligned}$$

Note that a deformed brick may not have planar faces since the first three points of a face determine a plane and the fourth corner vertex may not in general lie on this plane. Isoparametric coordinate mapping $(x(p,q,r), y(p,q,r), z(p,q,r))$ in (21) is affine if the hexahedral brick has parallel sides (and hence planar faces). Let the affine transformation be

$$\begin{bmatrix} x(p,q,r) \\ y(p,q,r) \\ z(p,q,r) \end{bmatrix} = \begin{bmatrix} u_x & v_x & w_x \\ u_y & v_y & w_y \\ u_z & v_z & w_z \end{bmatrix} \begin{bmatrix} p \\ q \\ r \end{bmatrix} + \begin{bmatrix} x_1 \\ y_1 \\ z_1 \end{bmatrix},$$

where

$$\begin{bmatrix} u_x \\ u_y \\ u_z \end{bmatrix} = \begin{bmatrix} x_2 - x_1 \\ y_2 - y_1 \\ z_2 - z_1 \end{bmatrix}, \quad \begin{bmatrix} v_z \\ v_y \\ v_z \end{bmatrix} = \begin{bmatrix} x_4 - x_1 \\ y_4 - y_1 \\ z_4 - z_1 \end{bmatrix}, \quad \begin{bmatrix} w_x \\ w_y \\ w_z \end{bmatrix} = \begin{bmatrix} x_5 - x_1 \\ y_5 - y_1 \\ z_5 - z_1 \end{bmatrix}.$$

The error term has the familiar form

$$\begin{aligned} E_Q(p,q,r) &= E_Q(p_c + dp, q_c + dq, r_c + dr) \\ &= p_\ell(p,q,r) - f(x(p,q,r), y(p,q,r), z(p,q,r)) \\ &= E_Q - \frac{1}{2}(\mu_1 dp^2 + \mu_2 dq^2 + \mu_3 dr^2) \end{aligned} \tag{23}$$

where

$$[p_c, q_c, r_c] = [1/2, 1/2, 1/2], \quad E_Q = E_Q(p_c, q_c, r_c) = \frac{1}{8}(\mu_1 + \mu_2 + \mu_3),$$

$$\begin{aligned} 0 &= \frac{\partial}{\partial p}E_Q(p_c,q_c,r_c) = \frac{\partial}{\partial q}E_Q(p_c,q_c,r_c) = \frac{\partial}{\partial r}E_Q(p_c,q_c,r_c)\,. \\ \mu_1 &= [u_x,u_y,u_z]H[u_x,u_y,u_z]^t, \quad \mu_2 = [v_x,v_y,v_z]H[v_x,v_y,v_z]^t, \\ \mu_3 &= [w_x,w_y,w_z]H[w_x,w_y,w_z]^t\,. \end{aligned} \tag{24}$$

For a convex data function ($\det(H) > 0$), maximum error is attained at the center $[p_c, q_c, r_c]$ and the optimal shape is a cube with an efficiency ratio of

$$\frac{\text{Error}}{\text{Volume}} = \frac{3L^2/8}{L^3} = \frac{3/8}{L} = \frac{3/8}{\sqrt{2}R/3} \approx 0.7955/R\,, \tag{25}$$

where $R = 3L/\sqrt{2}$ is the circum-radius.

For a saddle-shaped function ($\det(H) < 0$),

$$\begin{aligned} \mu_1 &= \tilde{u}_x^2 + \tilde{u}_y^2 - \tilde{u}_z^2, \quad \mu_2 = \tilde{v}_x^2 + \tilde{v}_y^2 - \tilde{v}_z^2 \\ \mu_3 &= \tilde{w}_x^2 + \tilde{w}_y^2 - \tilde{w}_z^2, \end{aligned}$$

over the isotropic space. The rotated brick with coordinates

$$\begin{aligned} [\tilde{u}_x,\tilde{u}_y,\tilde{u}_z] &= [L,0,L], \quad [\tilde{v}_x,\tilde{v}_y,\tilde{v}_z] = \left[-L/2,-\sqrt{3}L/2,L\right], \\ [\tilde{w}_x,\tilde{w}_y,\tilde{w}_z] &= \left[-L/2,\sqrt{3}L/2,L\right] \end{aligned} \tag{26}$$

has $\mu_1 = \mu_2 = \mu_3 = 0$ with maximal volume of $3\sqrt{3}/2L^3 \approx 2.598L^3$, hence is of optimal shape.

6.3. Comparison of bricks versus tetrahedrons

A similar result to Theorem 1 is available.

Theorem 2. *Any hexahedral parallelepiped over the isotropic space can be decomposed into six tetrahedrons with smaller maximum interpolation error for approximating a convex quadratic.*

A brick may be decomposed into six tetrahedrons by first splitting along a diagonal plane into two triangular prisms and then further partitioning the prism into three tetrahedrons. The proof involves careful consideration of 6 cases corresponding to different valid decompositions of a prism into 3 tetrahedrons and showing in each case tetrahedrons are more accurate than the brick. The details are contained in the Appendix.

7. Numerical Experiments

In this section, we demonstrate that a well designed mesh for bilinear interpolation of a saddle-shaped function may give substantial improvements over a triangular mesh. The examples are taken from [2]. The procedure in [2] for generating optimal triangular meshes is modified to generate optimal quadrilateral meshes. Only elements entirely interior to the unit square are generated to simplify the presentation.

Example 1. Exponential increase along x-axis,

$$f(x, y) = \exp(5x)\sin(5y) .$$

Example 2. A near singularity at $(x_0, y_0) = (0.5, -0.2)$,

$$f(x, y) = \frac{(x - x_0)^2 - (y - y_0)^2}{((x - x_0)^2 + (y - y_0)^2)^2} .$$

Example 3. A more severe near singularity,

$$f(x, y) = \frac{((x - x_0)^2 + (y - y_0)^2)^2 - 8(x - x_0)(^2(y - y_0)^2}{((x - x_0)^2 + (y - y_0)^2)^4} .$$

Example 4. Example 4 is Example 2 modified by a rescaling of y-axis,

$$f(x, y) = \frac{(x - x_0)^2 - (\sqrt{10}y - y_0)^2}{((x - x_0)^2 + (\sqrt{10}y - y_0)^2)^2} .$$

The results of the experiments are summarized in Figures 7–10 and Tables 1–4. Mesh I is generated by optimal squares over the isotropic space. Mesh II is generated by optimal squares with a $\pi/4$ rotation over the isotropic space to capture the "super-convergence" behavior. Both meshes have similar element size, element shape and density and differ mainly in their orientation. The meshes are displayed in Figures 11–18. Results for optimal triangular meshes produced in [2] are included for comparison. Mesh I produces an almost level error profile. This indicates an equilibration of interpolation error evenly over all elements. Error profile for Mesh I is roughly comparable to an optimal triangular mesh with about twice as many triangles and in agreement with discussions in §5. Mesh II displays the "super-convergence" behavior by consistently achieving an error 5–10 times smaller than Mesh I.

Table 5 shows the effect of generating finer meshes over the isotropic space. If we consider the median error, Mesh I shows the expected $O(h^2)$ convergence. From the efficiency ratio (Error / Area), we can also predict the decrease of error is proportional to the number of elements. Results for Mesh II clearly display the higher than $O(h^2)$ "super-convergence" be-

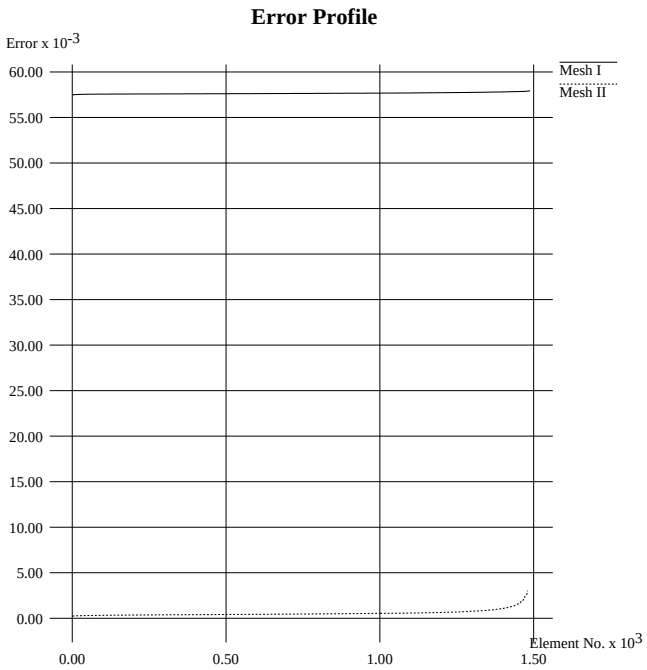

Figure 7: Error profiles for Example 1.

Table 1: Summary of results for Example 1.

	Minimum error	Median error	90 percentile	Maximum error	Number of elements
Triangle	5.27E-2	5.39E-2	5.50E-2	5.74E-2	2923
Mesh I	5.75E-2	5.76E-2	5.78E-2	5.79E-2	1488
Mesh II	2.29E-4	4.62E-4	8.30E-4	3.04E-3	1480

havior. From another perspective, about 5–10 times *more* elements are needed for Mesh I to match the accuracy of Mesh II.

It can be shown [1] that the coordinate lines in the isotropic space are mapped to eigen-trajectories of the Hessian matrix. Thus as the curved element boundaries are poorly approximated by straight edges, the resulting quadrilateral will no longer have parallel sides (Fig. 15, 16). The simple analysis for super-convergence in §3 for parallelograms may not be adequate and this leads to an anomalous increase in the error displayed in Example 3 of a severe singularity.

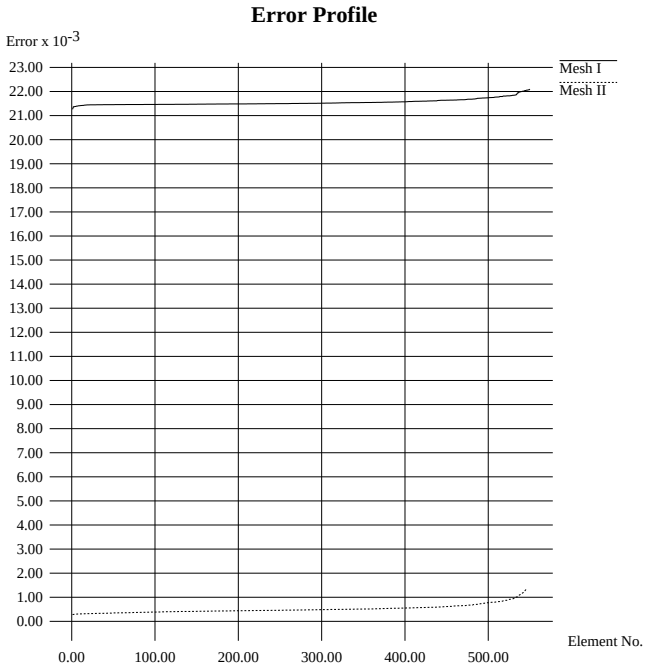

Figure 8: Error profiles for Example 2.

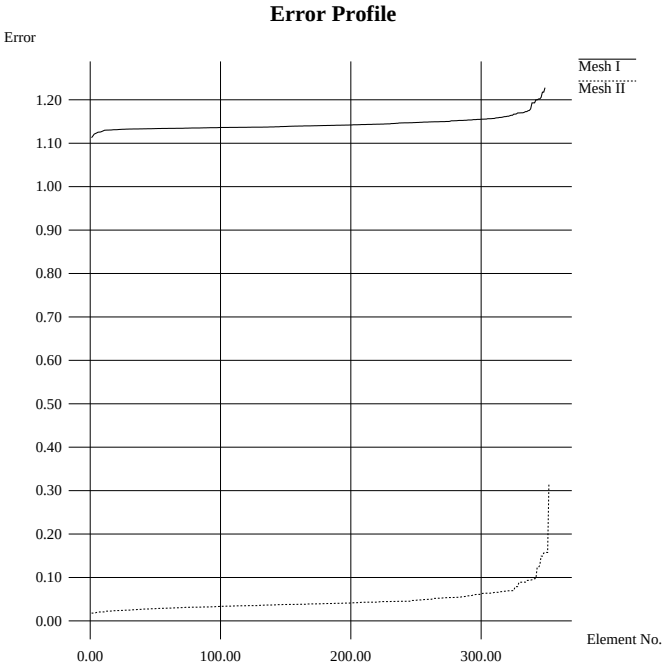

Figure 9: Error profiles for Example 2.

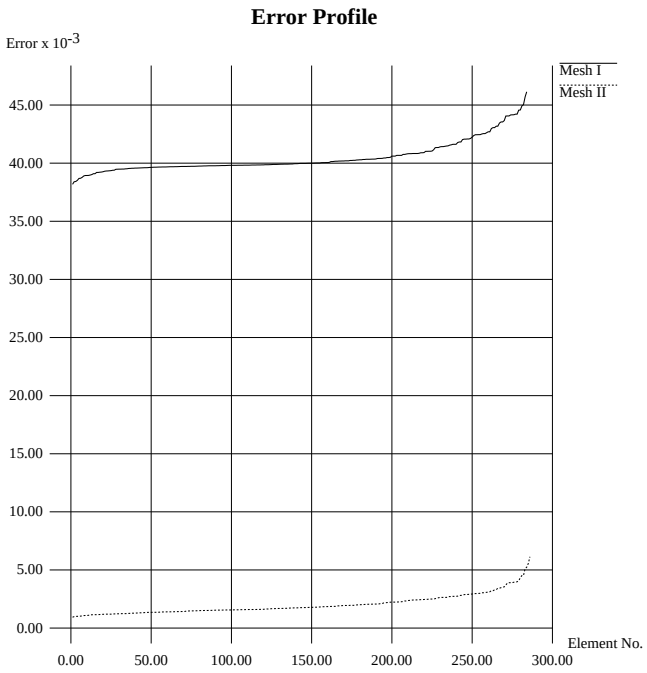

Figure 10: Error profiles for Example 3.

Table 2: Summary of results for Example 2.

	Minimum error	Median error	90 percentile	Maximum error	Number of elements
Triangle	1.87E-2	2.01E-2	2.16E-2	2.57E-2	1072
Mesh I	2.13E-2	2.15E-2	2.17E-2	2.21E-2	550
Mesh II	2.82E-4	4.69E-4	7.33E-4	1.38E-3	546

Table 3: Summary of results for Example 3.

	Minimum error	Median error	90 percentile	Maximum error	Number of elements
Triangle	1.02	1.16	1.32	1.70	650
Mesh I	1.11	1.14	1.16	1.23	349
Mesh II	1.80E-2	3.94E-2	6.75E-2	3.16E-1	352

Table 4: Summary of results for Example 4.

	Minimum error	Median error	90 percentile	Maximum error	Number of elements
Triangle	2.91E-2	3.68E-2	4.61E-2	6.46E-2	608
Mesh I	3.81E-2	4.00E-2	4.24E-2	4.61E-2	284
Mesh II	9.36E-4	1.76E-3	3.04E-3	6.13E-3	286

Table 5: Convergence test on Example 3.

	Minimum error	Median error	90 percentile	Maximum error	Number of elements
Mesh I	11.1E-1	11.4E-1	11.6E-1	12.3E-1	349
Mesh I	3.22E-1	3.23E-1	3.24E-1	3.26E-1	1223
Mesh I	8.03E-2	8.07E-2	8.12E-2	8.23E-2	5063
Mesh I	1.99E-2	2.02E-2	2.04E-2	2.08E-2	20603
Mesh II	1.80E-2	3.94E-2	6.75E-2	3.16E-1	352
Mesh II	2.35E-3	4.22E-3	9.16E-3	6.35E-2	1260
Mesh II	3.10E-4	7.20E-4	1.29E-3	9.41E-3	5244
Mesh II	5.19E-5	1.79E-4	3.78E-4	1.24E-3	21389

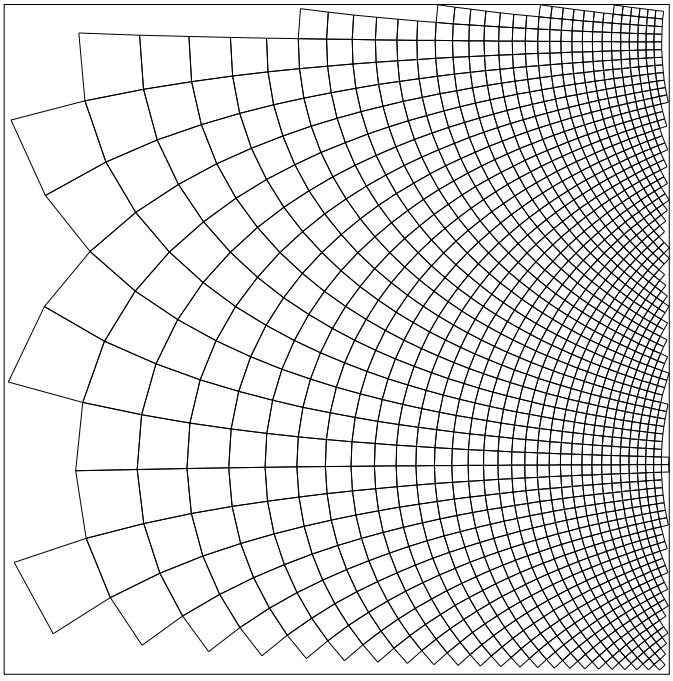

Figure 11: Mesh I for Example 1.

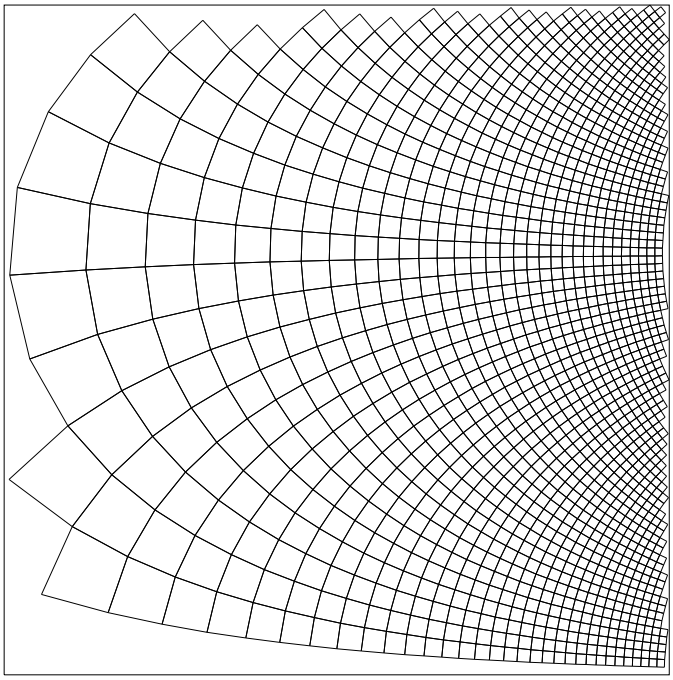

Figure 12: Mesh II for Example 1.

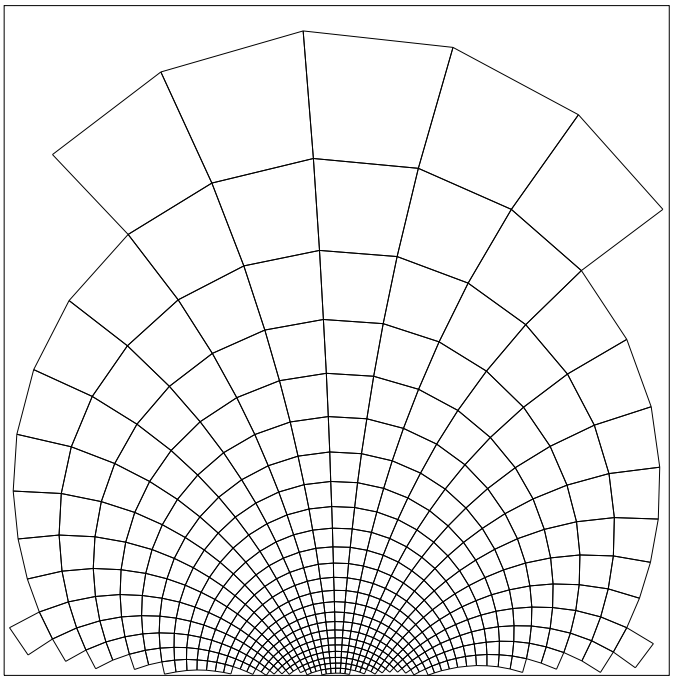

Figure 13: Mesh I for Example 2.

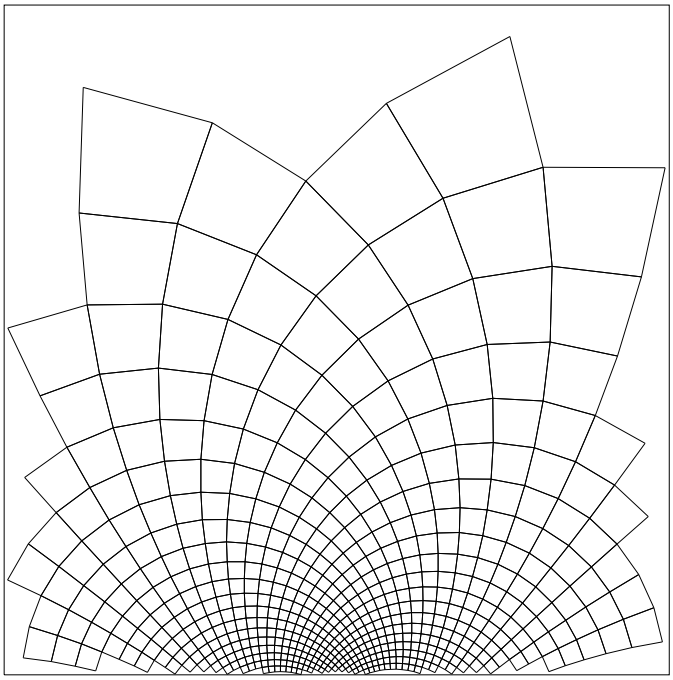

Figure 14: Mesh II for Example 2.

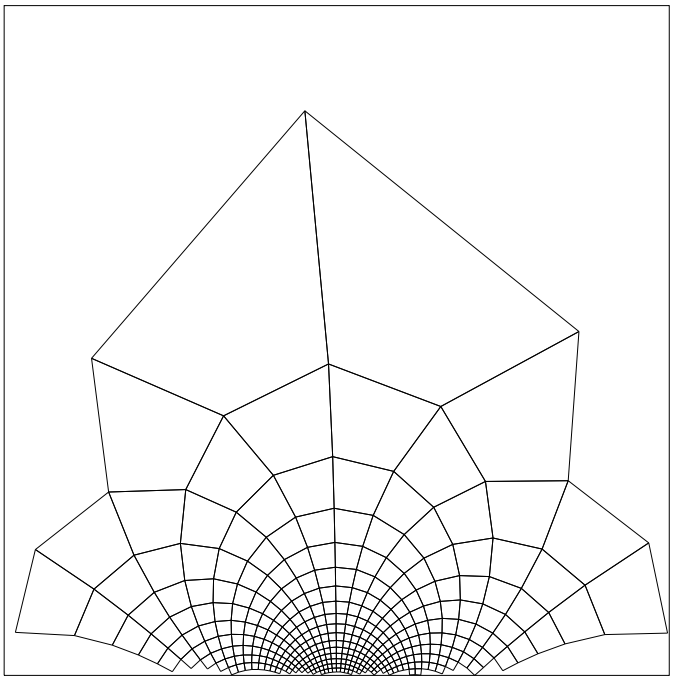

Figure 15: Mesh I for Example 3.

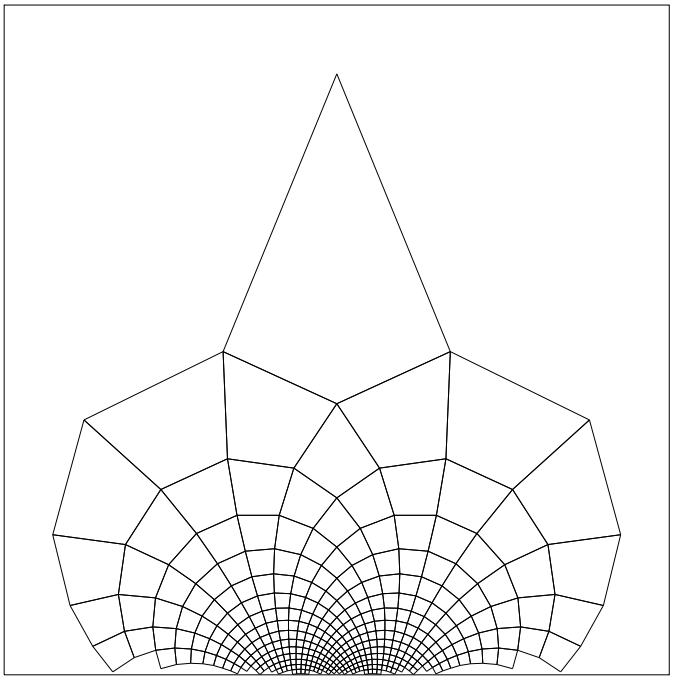

Figure 16: Mesh II for Example 3.

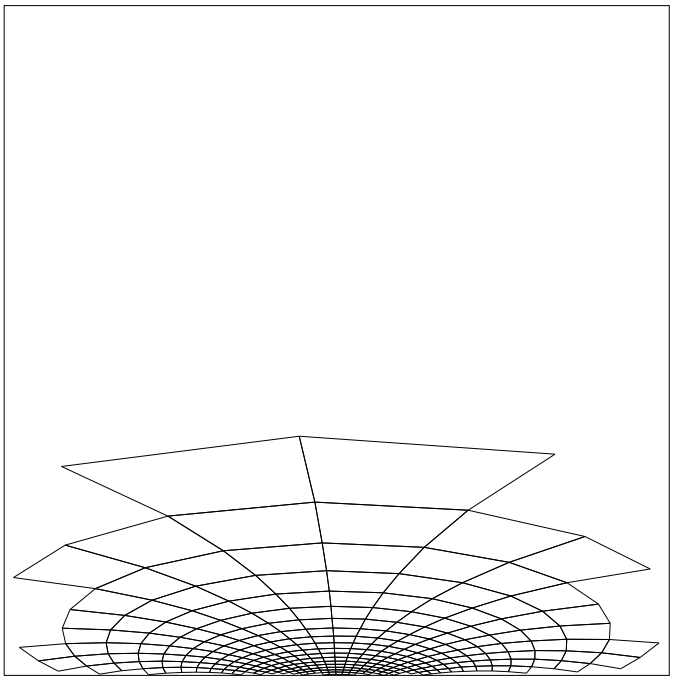

Figure 17: Mesh I for Example 4.

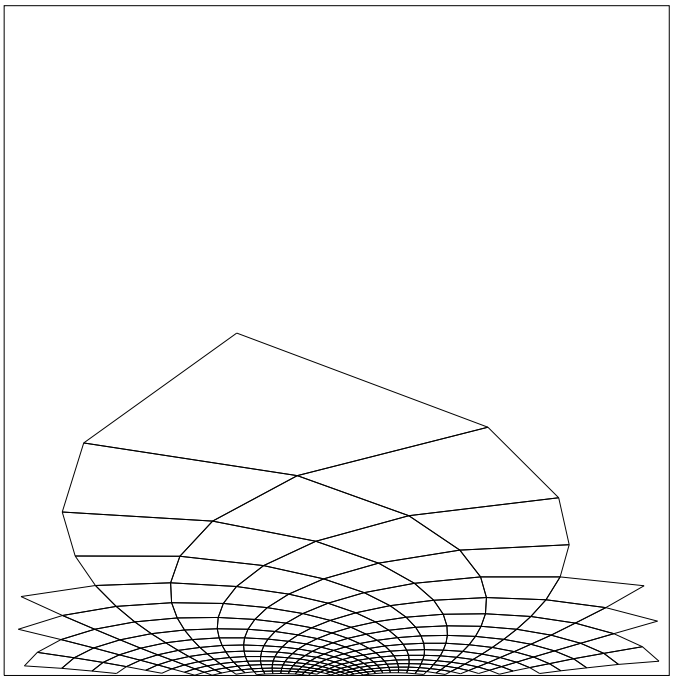

Figure 18: Mesh II for Example 4.

8. Summary

We have used a simple locally quadratic model to develop a geometric interpretation of the interpolation error. We determine the optimal element shapes and their efficiency ratio (Error / Area) over the isotropic space. The analysis shows for approximating convex data functions, although bilinear quadrilaterals are more efficient, linear triangles are more accurate and may be preferred in finite element computations. For approximating saddle-shaped data functions, a well designed quadrilateral mesh may show “super-convergence” improvements in approximation accuracy. Numerical experiments show good agreement with the analysis, and a surprising finding is different grid orientations may have an order of magnitude improvement in accuracy.

Appendix A

In this section, we show the error function for quadratic interpolation over a parallelogram is given by (10) by simple algebraic expansion. Let the data function be

$$f(x,y) \;=\; \frac{1}{2}[x,y]H[x,y]^t + [g_1,g_2][x,y]^t + c \tag{27}$$

and the affine isoparametric transformation be

$$\begin{bmatrix} x(p,q) \\ y(p,q) \end{bmatrix} \;=\; T\begin{bmatrix} p \\ q \end{bmatrix} + \begin{bmatrix} x_1 \\ y_1 \end{bmatrix},\; T = \begin{bmatrix} u_x & v_x \\ u_y & v_y \end{bmatrix} = \begin{bmatrix} x_2 - x_1 & x_4 - x_1 \\ y_2 - y_1 & y_4 - y_1 \end{bmatrix}. \tag{28}$$

Then the interpolation error can be shown to be

$$\begin{aligned} E_Q(p,q) &= p_\ell(x(p,q),y(p,q)) - f(x(p,q),y(p,q)) \\ &= E_Q - \frac{1}{2}\left(\mu_1(p-p_c)^2 + \mu_2(q-q_c)^2\right)\,, \end{aligned} \tag{29}$$

with centroid at $[p_c,q_c] = [\frac{1}{2},\frac{1}{2}]$,

$$\begin{aligned} E_Q &= E_Q(p_c,q_c) = \frac{1}{8}(\mu_1+\mu_2)\,, \\ \mu_1 &= [u_x,u_y]H[u_x,u_y]^t, \quad \mu_2 = [v_x,v_y]H[v_x,v_y]^t \end{aligned}$$

Let the data function over (p,q)-space be written as

$$\begin{aligned} \tilde{f}(p,q) &= f(x(p,q),y(p,q)) \\ &= \frac{1}{2}[p,q]\tilde{H}[p,q]^t + [\tilde{g}_1,\tilde{g}_2][p,q]^t + \tilde{c} \end{aligned}$$

$$\text{where } \tilde{H} = T^t H T = \begin{bmatrix} \tilde{h}_{11} & \tilde{h}_{12} \\ \tilde{h}_{12} & \tilde{h}_{22} \end{bmatrix} \quad \text{and} \tag{30}$$

$$\begin{aligned} [\tilde{g}_1,\tilde{g}_2] &= \left([g_1,g_2] + [x_1,y_1]H\right)T\,, \\ \tilde{c} &= c + [g_1,g_2][x_1,y_1]^t + \frac{1}{2}[x_1,y_1]H[x_1,y_1]^t\,. \end{aligned} \tag{31}$$

The function values at the four interpolating corners are

$$f_1 \;=\; \tilde{f}(0,0) = \tilde{c}\,, \quad f_3 = \tilde{f}(1,1) = \frac{1}{2}(\tilde{h}_{11}+\tilde{h}_{22}+2\tilde{h}_{12}) + \tilde{g}_1 + \tilde{g}_2 + \tilde{c}\,, \tag{32}$$

$$f_2 \quad = \quad \tilde{f}(1,0) = \frac{1}{2}\tilde{h}_{11} + \tilde{g}_1 + \tilde{c}\,, \quad f_4 = \tilde{f}(0,1) = \frac{1}{2}\tilde{h}_{22} + \tilde{g}_2 + \tilde{c}\,.$$

By (9) and (29) (note the vanishing of linear and constant terms),

$$\begin{aligned} E_Q(p,q) &= \left(\sum_{i=1}^{i=4} f_i\phi_i(p,q)\right) - \tilde{f}(p,q) \\ &= \frac{1}{2}\left(p(1-q)\tilde{h}_{11} + pq(\tilde{h}_{11} + \tilde{h}_{22} + 2\tilde{h}_{12})\right. \\ &\qquad \left. +(1-p)q\tilde{h}_{22} - (p^2\tilde{h}_{11} + q^2\tilde{h}_{22} + 2pq\tilde{h}_{12})\right) \\ &= \frac{1}{2}\left(p\tilde{h}_{11} + q\tilde{h}_{22} + 2pq\tilde{h}_{12} - p^2\tilde{h}_{11} - q^2\tilde{h}_{22} - 2pq\tilde{h}_{12}\right) \\ &= \frac{1}{2}\left(p(1-p)\tilde{h}_{11} + q(1-q)\tilde{h}_{22}\right) \\ &= \frac{1}{8}(\tilde{h}_{11} + \tilde{h}_{22}) - \frac{1}{2}(\tilde{h}_{11}(p-\frac{1}{2})^2 + \tilde{h}_{22}(q-\frac{1}{2})^2)\,. \end{aligned} \tag{33}$$

From (28) and (30), we have $\tilde{h}_{11} = \mu_1$ and $\tilde{h}_{22} = \mu_2$; hence the error function has the form given in (29).

Appendix B

In this section, we show that any hexahedral parallelepiped over the isotropic space can be decomposed into six tetrahedrons with smaller maximum interpolation error approximating a convex quadratic. The two-dimensional analogue is to decompose a parallelogram into two triangles using the diagonal sustained at an acute angle. This criterion also corresponds to a Delauney triangulation that maximizes the smaller angle in the triangulation.

The decomposition we propose for the brick is based on examining each face, which is a parallelogram, and selecting the cut diagonal based on the above Delauney criterion in two-dimensions. We recall from §6.1 the maximum error for a tetrahedron is bounded above by $L^2/8$ where L is length of longest edge, and the error for the brick is $(L_1^2 + L_2^2 + L_3^2)/8$. Through a detailed case by case analysis we shall show the longest edge L in any *valid* decomposition into tetrahedrons is less than sqrt$(L_1^2 + L_2^2 + L_3^2)$.

Proof. By symmetry considerations, and without loss in generality, we shall examine only the triangular prism oriented with the longest side along the x-axis (see Figure 19) with $\angle CAB$ an acute angle, where

$$\begin{aligned} L_1 = |AB| = |DE| &\geq |AC| = |DF| = \sqrt{s^2 + t^2} = L_2 \\ &\geq |AD| = |BE| = |CF| = \sqrt{x^2 + y^2 + z^2} = L_3\,. \end{aligned} \tag{34}$$

We examine the three parallelogram faces to determine the appropriate diagonal cuts, and

in each case we can show the diagonal edge chosen has length less than sqrt($L_1^2 + L_2^2 + L_3^2$). Since edge $|CB| = |FE|$ has length and $\theta \leq \pi/2$ is acute by choice,

$$|CB|^2 = L_1^2 + L_2^2 - 2L_1L_2\cos(\theta) \leq L_1^2 + L_2^2 + L_3^2 \,.$$

Condition 1. Consider the face $ABED$, $\angle DAB$ is acute if the dot product of AD and AB is positive. Thus,

$$\angle DAB \leq \pi/2 \quad \text{if } xL_1 \geq 0. \tag{35}$$

Note edge lengths are

$$\begin{aligned} |AE|^2 &= (x+L_1)^2 + y^2 + z^2 = L_1^2 + L_3^2 + 2(xL_1) \\ |DB|^2 &= (x-L_1)^2 + y^2 + z^2 = L_1^2 + L_3^2 - 2(xL_1) \end{aligned} \tag{36}$$

If $\angle DAB$ is acute ($xL_1 \geq 0$), diagonal edge DB is selected and $|DB|^2 < L_1^2 + L_3^2$; otherwise ($xL_1 < 0$), diagonal edge AE is selected and $|AE|^2 < L_1^2 + L_3^2$.

Condition 2. Consider the face $CBEF$, $\angle FCB$ is acute if the dot product of CF and CB is positive. Thus,

$$\angle FCB \leq \pi/2 \quad \text{if } x(L_1 - s) + y(-t) + z(0) \geq 0, \text{ or } xL_1 \geq xs + yt. \tag{37}$$

Note edge lengths are

$$\begin{aligned} |CE|^2 &= ((x+L_1)-s)^2 + (y-t)^2 + z^2 \\ &= L_1^2 + L_2^2 + L_3^2 + 2((xL_1 - xs - yt) - sL_1) \\ |FB|^2 &= ((x+s)-L_1)^2 + (y+t)^2 + z^2 \\ &= L_1^2 + L_2^2 + L_3^2 - 2((xL_1 - xs - yt) + sL_1) \end{aligned} \tag{38}$$

If $\angle FCB$ is acute ($xL_1 \geq xs + yt$), diagonal edge FB is chosen and $|FB|^2 < L_1^2 + L_2^2 + L_3^2$; otherwise ($xL_1 < xs + yt$), diagonal edge CE is chosen and $|CE|^2 < L_1^2 + L_2^2 + L_3^2$.

Condition 3. Consider the face $ACFD$, $\angle DAC$ is acute if the dot product of AD and AC is positive. Thus,

$$\angle DAC \leq \pi/2 \quad \text{if } xs + yt \geq 0. \tag{39}$$

Note edge lengths are

$$|AF|^2 = (x+s)^2 + (y+t)^2 + z^2 = L_1^2 + L_2^2 + L_3^2 + 2(xs + yt)$$

$$|DC|^2 \quad = \quad (x-s)^2 + (y-t)^2 + z^2 = L_1^2 + L_2^2 + L_3^2 - 2(xs+yt) \tag{40}$$

If $\angle DAC$ is acute ($xs+yt \geq 0$), diagonal edge DC is chosen and $|DC|^2 < L_1^2 + L_2^2 + L_3^2$; otherwise ($xs+yt < 0$), diagonal edge AF is chosen and $|AF|^2 < L_1^2 + L_2^2 + L_3^2$.

We shall consider different configurations for Conditions 1–3. For convenience, let the notation $[T, F, T]$ denote the case Conditions 1 and 3 are true, and Condition 2 is false, i.e. $\angle DAB \leq \pi/2$, $\angle FCB > \pi/2$, $\angle DAC \leq \pi/2$. We observe Conditions 2 and 3 imply Condition 1,

$$xL_1 \geq xs + yt \text{ and } xs + yt \geq 0 \text{ imply } xL_1 \geq 0. \tag{41}$$

Thus $[F, T, T]$ is impossible. By similar arguments, $[T, F, F]$ is impossible,

$$xL_1 < xs + yt \text{ and } xs + yt < 0 \text{ imply } xL_1 < 0. \tag{42}$$

Figures 20–27 display all eight possible cases for Conditions 1–3. Impossible cases $[T, F, T]$ and $[F, T, T]$ are shown to be associated with invalid decompositions. In all the six valid cases, the longest edge is less than sqrt($L_1^2 + L_2^2 + L_3^2$), hence the maximum error attained for tetrahedrons is smaller than the error for the hexahedral brick.

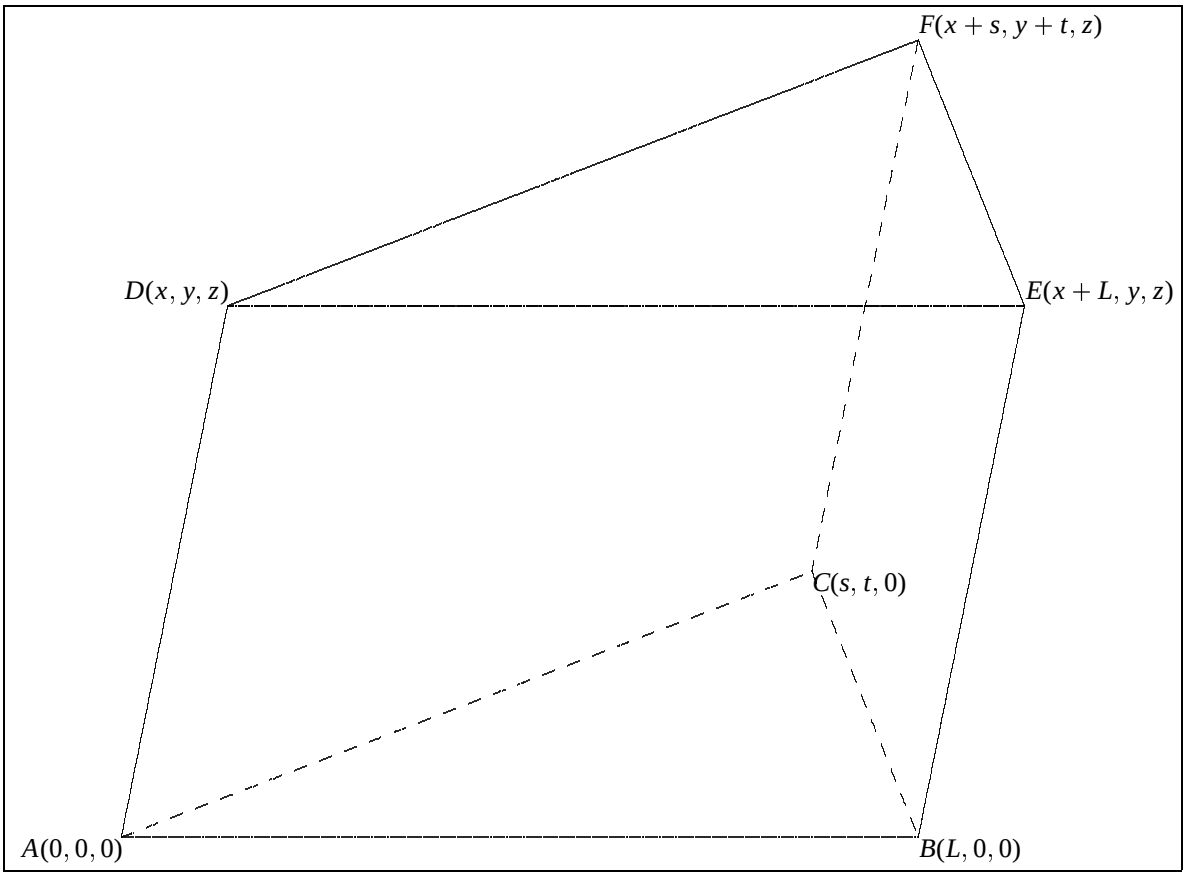

Figure 19: Prism.

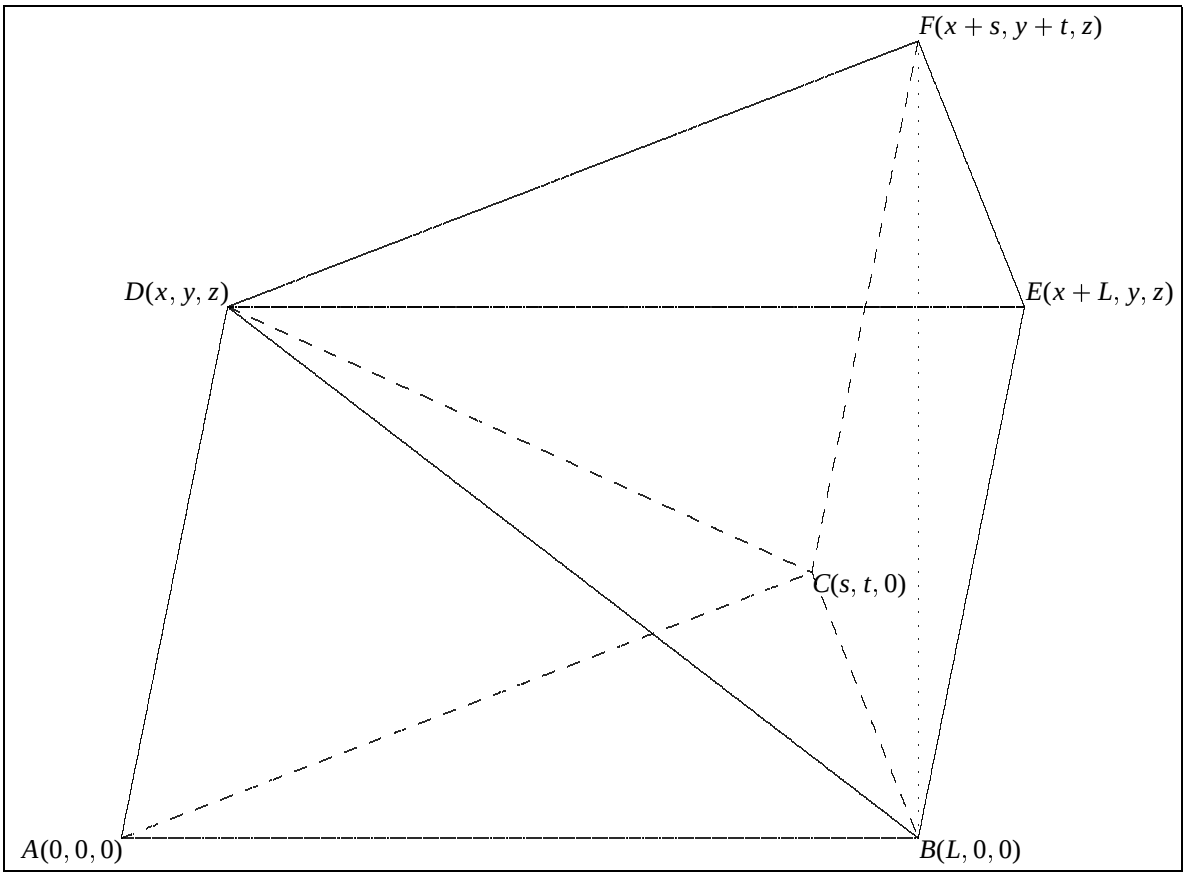

Figure 20: [T,T,T]. Valid decomposition.

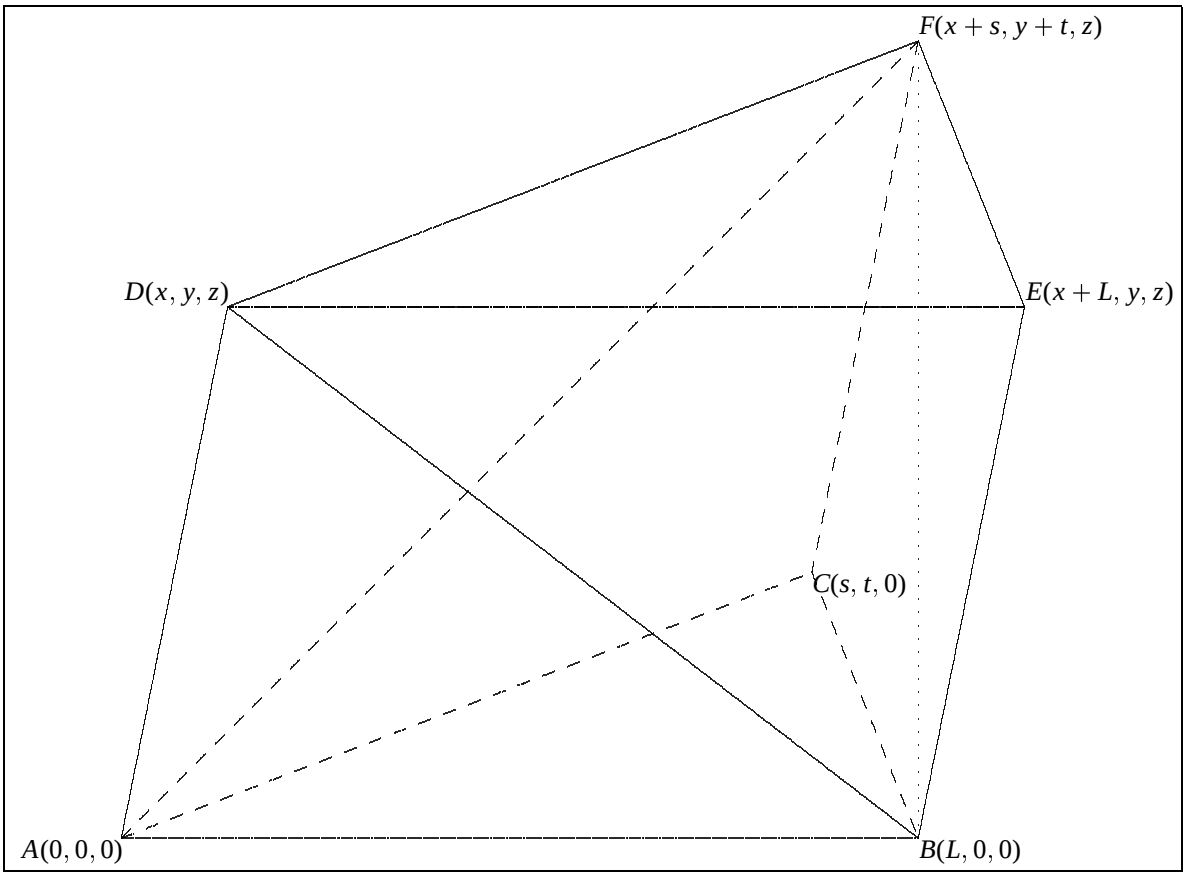

Figure 21: [T,T,F]. Valid decomposition.

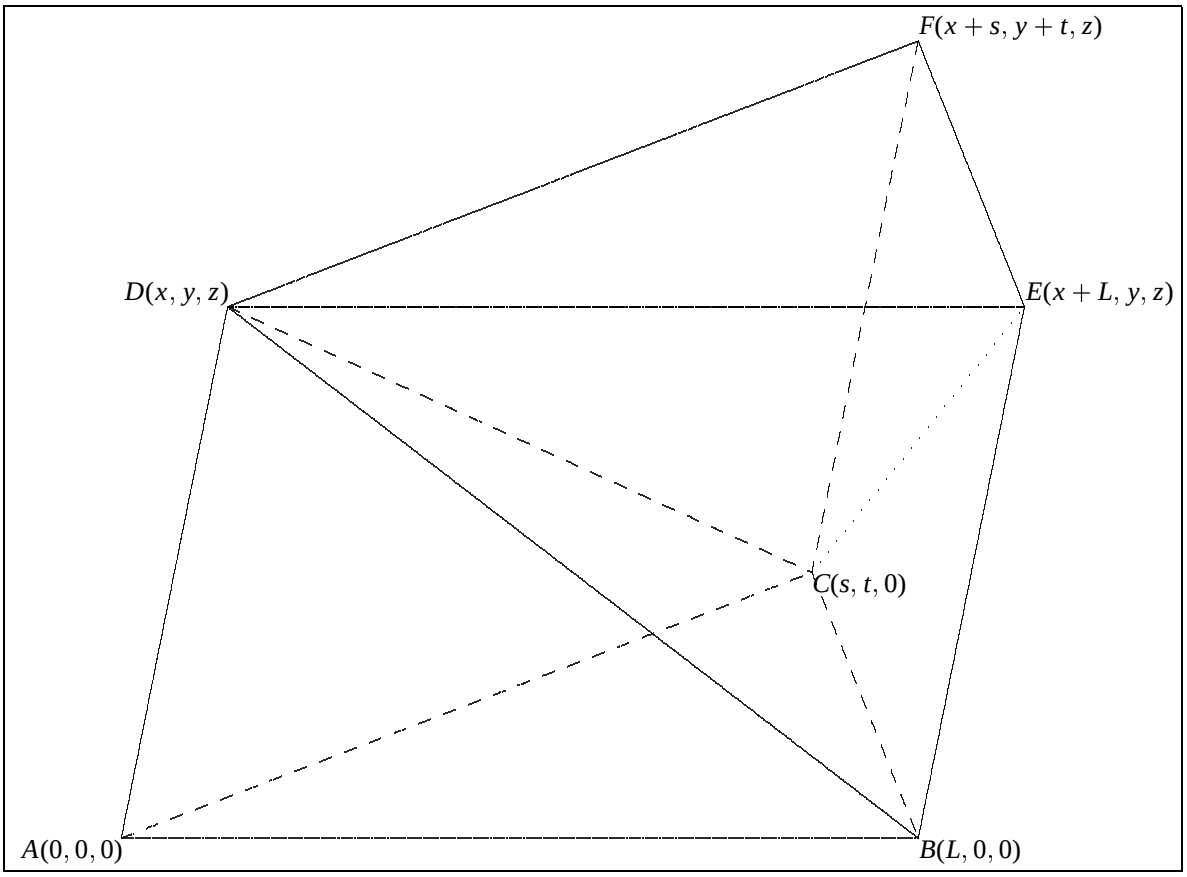

Figure 22: [T,F,T]. Valid decomposition.

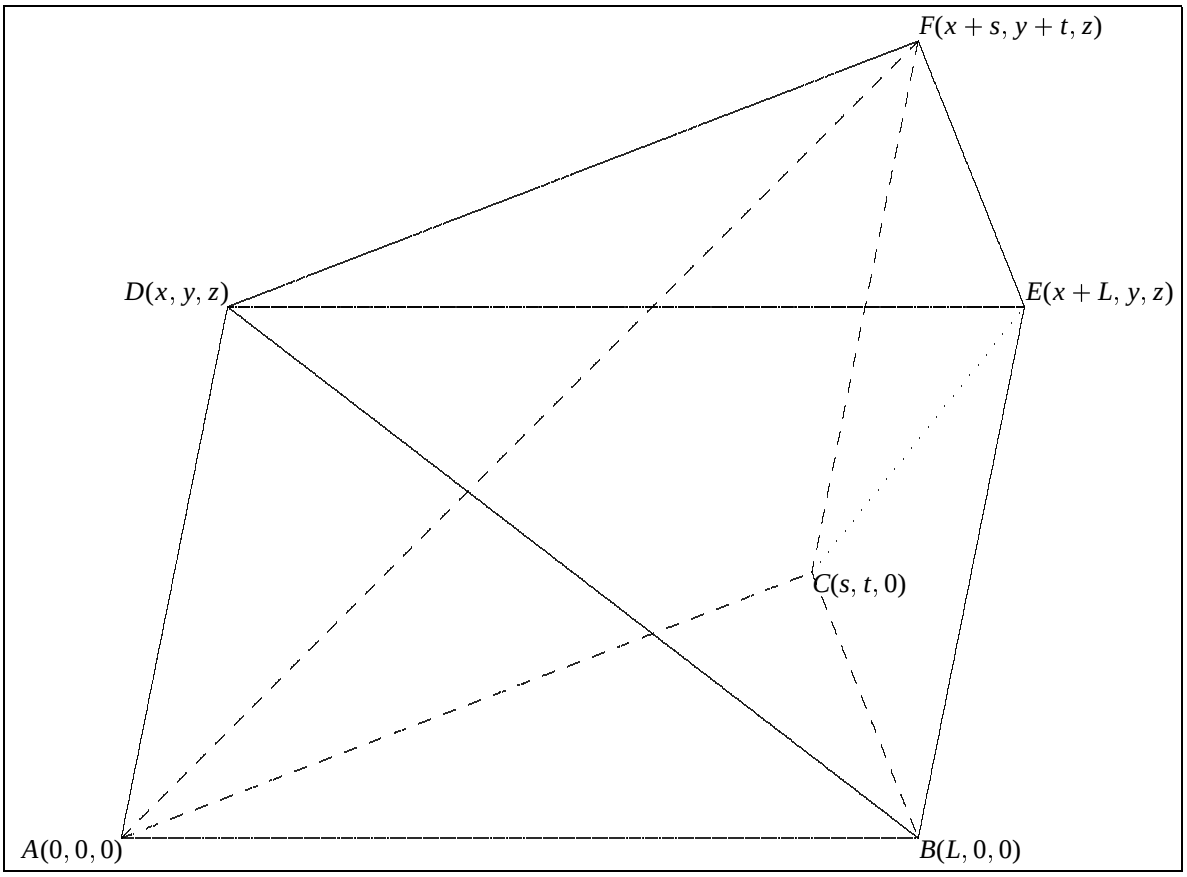

Figure 23: [T,F,F]. Invalid decomposition.

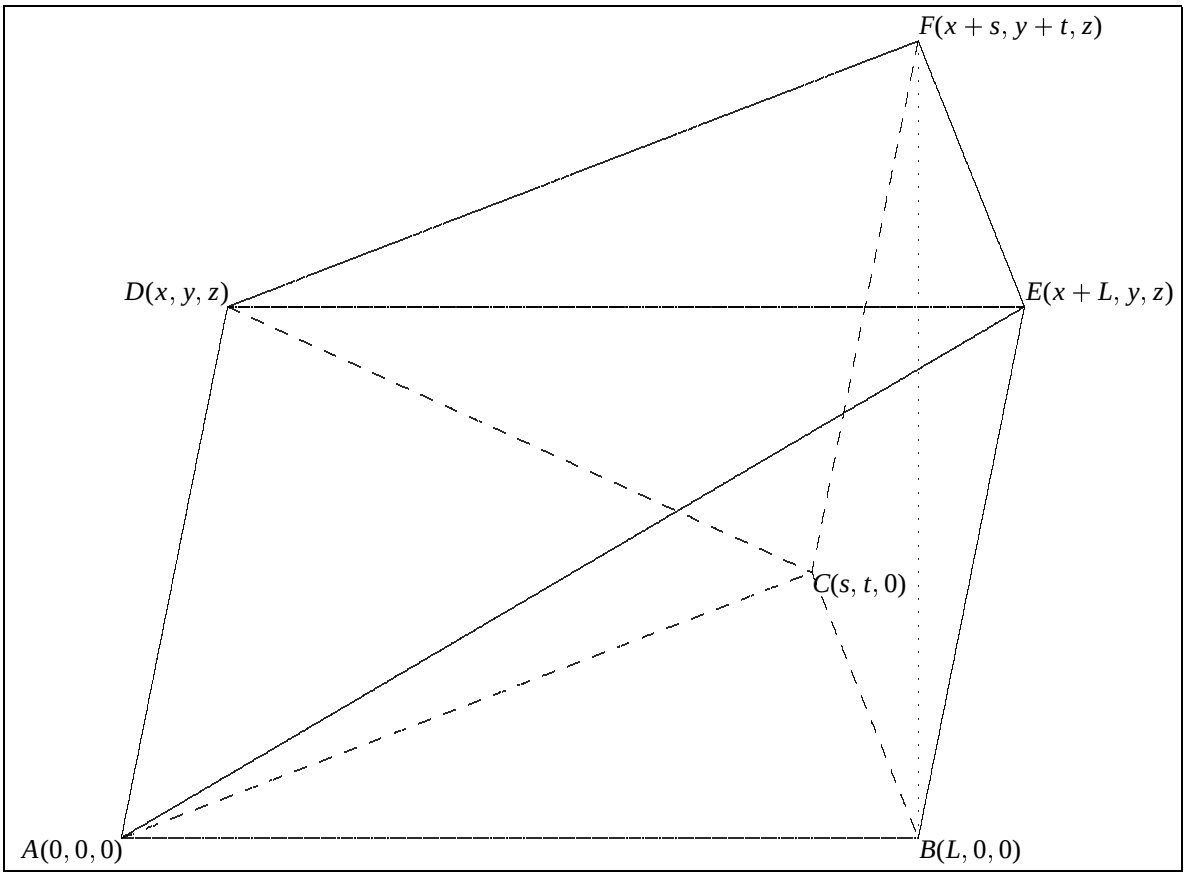

Figure 24: [F,T,T]. Invalid decomposition.

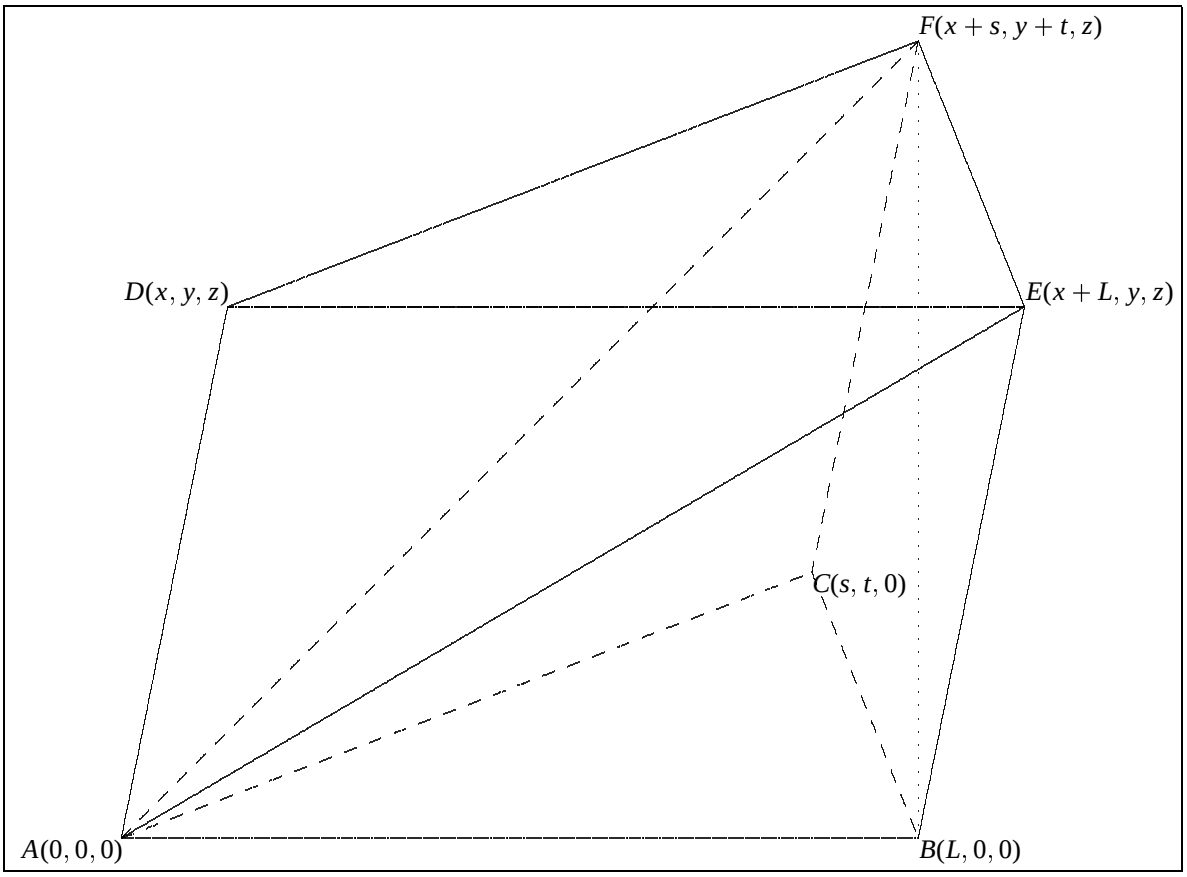

Figure 25: [F,T,F]. Valid decomposition.

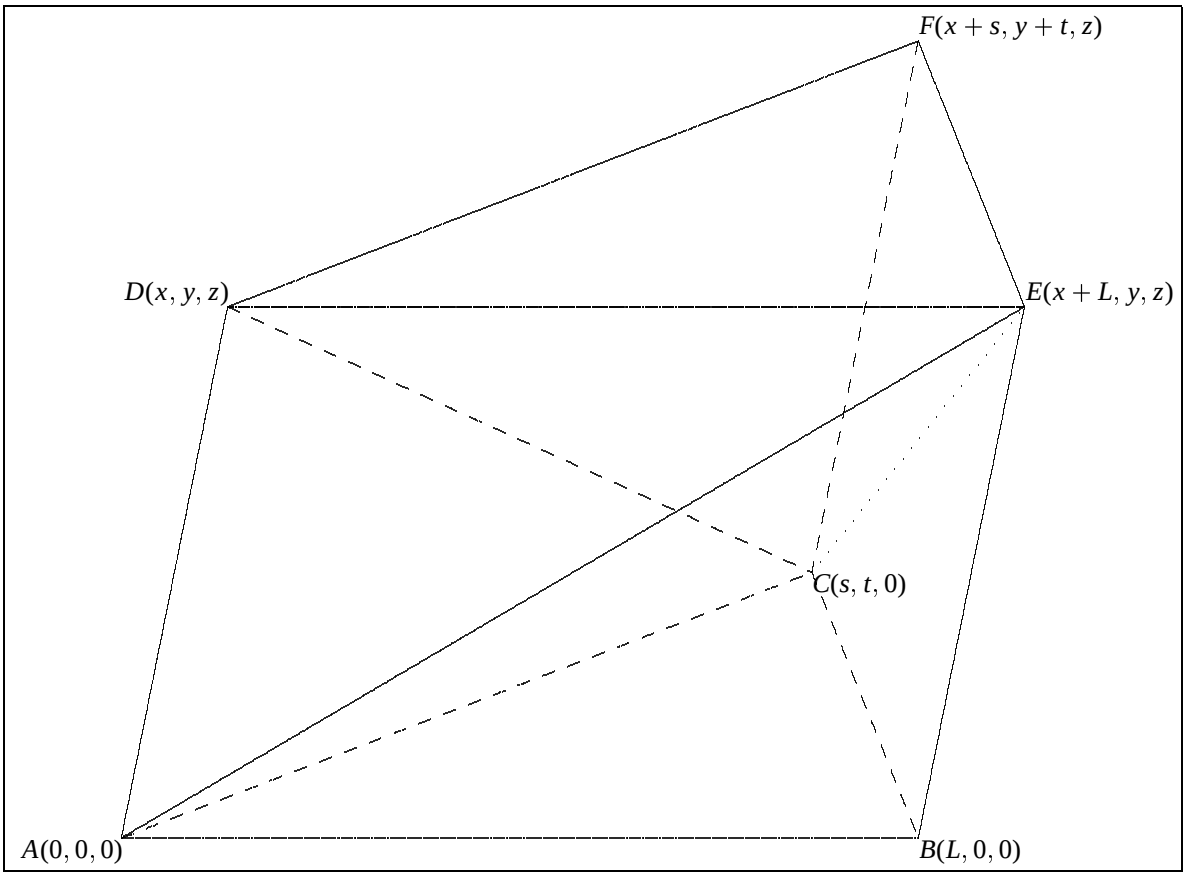

Figure 26: [F,F,T]. Valid decomposition.

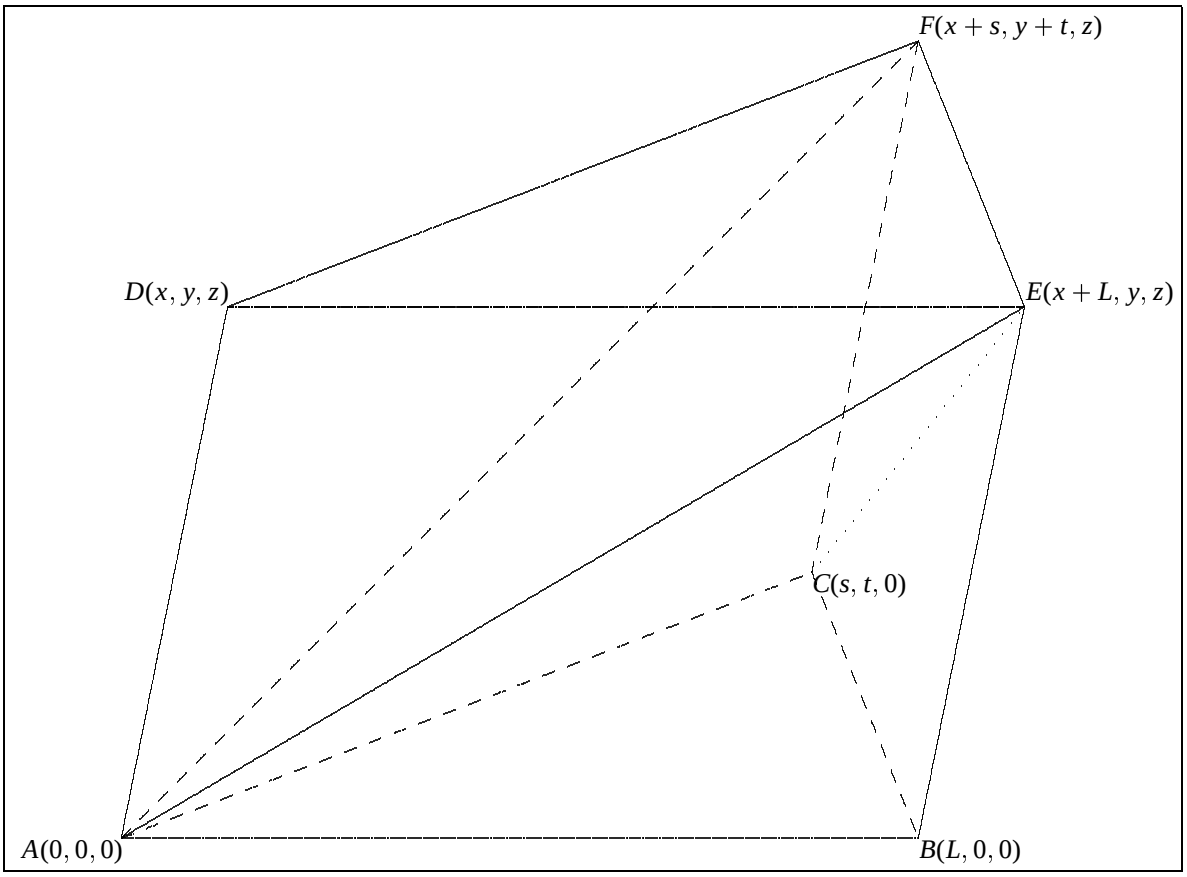

Figure 27: [F,F,F]. Valid decomposition.

9. References

[1] E. F. D'Azevedo. *On Optimal Triangulation for Piecewise Linear Approximation.* PhD thesis, Department of Computer Science, University of Waterloo, Waterloo, Ontario, Canada, 1989.

[2] E. F. D'Azevedo. Optimal triangular mesh generation by coordinate transformation. *SIAM J. Sci. Statist. Comput.*, 12(4):755–786, 1991.

[3] E. F. D'Azevedo and R. B. Simpson. On optimal interpolation incidences. *SIAM J. Sci. Statist. Comput.*, 10:1063–1075, 1989.

[4] E. F. D'Azevedo and R. B. Simpson. On optimal triangular meshes for minimizing the gradient error. *Numer. Math.*, 59:321–348, 1991.

[5] A. R. Mitchell and R. Wait. *The Finite Element Methods in Partial Differential Equations.* Wiley-Interscience Publication, 1977.

[6] Douglas William Moore. *Simplical Mesh Generation With Application.* PhD thesis, Cornell University, Ithaca, New York, 1992.

[7] E. Nadler. Piecewise linear best l_2 approximation on triangulations. In C. K. Chui, L. L. Schumaker, and J. D. Ward, editors, *Approximation Theory V*, pages 499–502, Boston, 1986. Academic Press.

[8] J. Peraire, M. Vahdati, K Morgan, and O. C. Zienkiewics. Adaptive remeshing for compressible flow computations. *J. Comput. Phys.*, 72:449–466, 1987.

[9] R. B. Simpson. Anisotropic mesh transformations and optimal error control. *Applied Numerical Mathematics*, 1992. Speical issue as the proceedings of the US Army sponsored Workshop for Adaptive Methods for Partial Differential Equations, Rensselaer Polytechnical Institute (accepted).

[10] W. D. Smith. *Studies in Discrete and Computational Geometry.* PhD thesis, Princeton University, 1988.

[11] I. S. Sokolnikoff. *Tensor Analysis, Theory and Applications to Geometry and Mechanics of Continua.* John Wiley, New York, second edition, 1964.

[12] G. van der Laan and A. J. J. Talman. An improvement of fixed point algorithms by using a good triangulation. *Mathematical Programming*, 18:274–285, 1980.

ORNL/TM-12388

INTERNAL DISTRIBUTION

1. V. Alexiades
2. B. R. Appleton
3–4. T. S. Darland
5–9. E. F. D'Azevedo
10. J. B. Drake
11. R. E. Flanery
12. C. E. Oliver
13–17. S. A. Raby
18–22. R. F. Sincovec
23–27. R. C. Ward
28. D. W. Walker
29. Central Research Library
30. ORNL Patent Office
31. K-25 Applied Technology Library
32. Y-12 Technical Library
33. Laboratory Records - RC
34–35. Laboratory Records Department

EXTERNAL DISTRIBUTION

36. Christopher R. Anderson, Department of Mathematics, University of California, Los Angeles, CA 90024

37. I. Babuska, Department of Mathematics and the Institute for Physical Science and Technology, University of Maryland, College Park, MD 20742

38. David C. Bader, Atmospheric and Climate Research Division, Office of Health and Environmental Research, Office of Energy Research, ER-76, U.S. Department of Energy, Washington, DC 20585

39. David H. Bailey, NASA Ames, Mail Stop 258-5, NASA Ames Research Center, Moffet Field, CA 94035

40. Dr. R. E. Bank, University of California / San Diego, Department of Mathematics, C-012, La Jolla, CA 92093

41. Edward H. Barsis, Computer Science and Mathematics, P. O. Box 5800, Sandia National Laboratory, Albuquerque, NM 87185

42. Colin Bennett, Department of Mathematics, University of South Carolina, Columbia, SC 29208

43. Dominique Bennett, CERFACS, 42 Avenue Gustave Coriolis, 31057 Toulouse Cedex, FRANCE

44. Marsha J. Berger, Courant Institute of Mathematical Sciences, 251 Mercer Street, New York, NY 10012

45. Mike Berry, Department of Computer Science, University of Tennessee, 107 Ayres Hall, Knoxville, TN 37996-1301

46. Ake Bjorck, Department of Mathematics, Linkoping University, S-581 83 Linkoping, Sweden

47. John H. Bolstad, Lawrence Livermore National Laboratory, L-16, P. O. Box 808, Livermore, CA 94550

48. George Bourianoff, Superconducting Super Collider Laboratory, 2550 Beckleymeade Avenue, Suite 260, Dallas, TX 75237-3946

49. Roger W. Brockett, Wang Professor of EE and CS, Division of Applied Sciences, Harvard University, Cambridge, MA 02138

50. Bill L. Buzbee, Scientific Computing Division, National Center for Atmospheric Research, P.O. Box 3000, Boulder, CO 80307

51. Captain Edward A. Carmona, Parallel Computing Research Group, U. S. Air Force Weapons Laboratory, Kirtland AFB, NM 87117

52. Peter Campbell, Environmental Science Division, Argonne National Laboratory, 9700 South Cass Avenue, Argonne, IL 60439

53. Dr. Jose Castillo, Department of Mathematical Sciences, San Diego State University, San Diego, CA 92182

54. John Cavallini, Acting Director, Scientific Computing Staff, Applied Mathematical Sciences, Office of Energy Research, U.S. Department of Energy, Washington, DC 20585

55. Professor I-Liang Chern, Department of Mathematics, National Taiwan University, Taipei, Taiwan, R.O.C.

56. Ray Cline, Sandia National Laboratories, Livermore, CA 94550

57. Alexandre Chorin, Mathematics Department, Lawrence Berkeley Laboratory, Berkeley, CA 94720

58. James Corones, Ames Laboratory, Iowa State University, Ames, IA 50011

59. Jean Coté, RPN, 2121 Transcanada Highway, Suite 508, Dorval, Quebec H9P 1J3, CANADA

60. William Dannevik, Lawrence Livermore National Laboratory, P. O. Box 808, L-16, Livermore, CA 94550

61. John J. Dorning, Department of Nuclear Engineering Physics, Thornton Hall, McCormick Road, University of Virginia, Charlottesville, VA 22901

62. Donald J. Dudziak, Department of Nuclear Engineering, 110B Burlington Engineering Labs, North Carolina State University, Raleigh, NC 27695-7909

63. Iain S. Duff, Atlas Centre, Rutherford Appleton Laboratory, Didcot, Oxon OX11 0QX, England

64. John Dukowicz, Los Alamos National Laboratory, Group T-3, Los Alamos, NM 87545

65. Richard E. Ewing, Department of Mathematics, Texas A&M University, College Station, TX 77843

66. Gerald Farin, Department of Computer Science, Arizona State University, Temple, AZ 85287

67. Joseph Flaherty, Department of Computer Science, Rensselaer Polytechnic Institute, Troy, New York 12180–3590

68. Ian Foster, Mathematics and Computer Science Division, Argonne National Laboratory, 9700 South Cass Avenue, Argonne, IL 60439

69. Geoffrey C. Fox, NPAC, 111 College Place, Syracuse University, Syracuse, NY 13244-4100

70. Dr. R. Francis, Div. of Information Technology, CSIRO, 723 Swanston Street, Carlton, Vic. 3053, AUSTRALIA

71. Paul O. Frederickson, ACL, MS B287, Los Alamos National Laboratory, Los Alamos, NM 87545

72. J. Alan George, Vice President, Academic and Provost, Needles Hall, University of Waterloo, Waterloo, Ontario, CANADA N2L 3G1

73. James Glimm, Department of Mathematics, State University of New York, Stony Brook, NY 11794

74. Gene Golub, Computer Science Department, Stanford University, Stanford, CA 94305

75. John Gustafson, 236 Wilhelm, Ames Laboratory, Iowa State University, Ames, IA 50011

76. Phil Gresho, Lawrence Livermore National Laboratory, L-262, P. O. Box 808, Livermore, CA 94550

77. William D. Gropp, Mathematics and Computer Science Division, Argonne National Laboratory, 9700 South Cass Avenue, Argonne, IL 60439

78. Eric Grosse, AT&T Bell Labs 2T-504, Murray Hill, NJ 07974

79. James J. Hack, National Center for Atmospheric Research, P. O. Box 3000, Boulder, CO 80307

80. Michael T. Heath, Center for Supercomputing Research and Development, 305 Talbot Laboratory, University of Illinois, 104 South Wright Street, Urbana, IL 61801-2932

81. Michael Henderson, Los Alamos National Laboratory, Group T-3, Los Alamos, NM 87545

82. Dr. Fred Howes, Office of Scientific Computing, ER-7, Applied Mathematical Sciences, Office of Energy Research, U. S. Department of Energy, Washington, DC 20585

83. Dr. Barry Joe, Department of Computer Science, University of Alberta, Edmonton, Alberta, Canada T6G 2H1

84. Dr. Gary Johnson, Office of Scientific Computing, ER-7, Applied Mathematical Sciences, Office of Energy Research, U. S. Department of Energy, Washington, DC 20585

85. Lennart Johnsson, Thinking Machines Inc., 245 First Street, Cambridge, MA 02142-1214

86. J. Jortner, Sandia National Labs, Division 1424, P.O. Box 5800, Albuquerque, NM 87185

87. J.R. Jump, ECE Dept., Rice University, P.O. Box 1892, Houston, TX 77251

88. Malvyn Kalos, Cornell Theory Center, Engineering and Theory Center Bldg., Cornell University, Ithaca, NY 14853-3901

89. Hans Kaper, Mathematics and Computer Science Division, Argonne National Laboratory, 9700 South Cass Avenue, Argonne, IL 60439

90. Alan H. Karp, IBM Scientific Center, 1530 Page Mill Road, Palo Alto, CA 94304

91. Kenneth Kennedy, Department of Computer Science, Rice University, P. O. Box 1892, Houston, Texas 77001

92. Tom Kitchens, ER-7, Applied Mathematical Sciences, Scientific Computing Staff, Office of Energy Research, Office G-437 Germantown, Washington, DC 20585

93. Peter D. Lax, Courant Institute of Mathematical Sciences, New York University, 251 Mercer Street, New York, NY 10012

94. James E. Leiss, Rt. 2, Box 142C, Broadway, VA 22815

95. Rich Loft, National Center for Atmospheric Research, P. O. Box 3000, Boulder, CO 80307

96. Michael C. MacCracken, Lawrence Livermore National Laboratory, L-262, P. O. Box 808, Livermore, CA 94550

97. Norman D. Malmuth, Science Center, Rockwell International Corporation, 1049 Camino Dos Rios, P.O. Box 1085, Thousand Oaks, CA 91358

98. Robert Malone, C-DO/ACL, MS B287, Los Alamos National Laboratory, Los Alamos, NM 87545

99. Len Margolin, Los Alamos National Laboratory, Los Alamos, NM 87545

100. Hal Marshall Laboratory for Scientific Computation, Rm. 271 Cooley Bld., University of Michigan, Ann Arbor, MI 48109-2104

101. Dr. Wayne Mastin, Department of Mathematics, Drawer A, Mississippi State University, Mississippi State, Mississippi 39762

102. Frank McCabe, Department of Computing, Imperial College of Science and Technology, 180 Queens Gate, London SW7 2BZ, ENGLAND

103. James McGraw, Lawrence Livermore National Laboratory, L-306, P. O. Box 808, Livermore, CA 94550

104. L. David Meeker, Mathematics Department, University of New Hampshire, Kingsbury Hall, Durham, NH 03824

105. Paul C. Messina, Mail Code 158-79, California Institute of Technology, 1201 E. California Blvd. Pasadena, CA 91125

106. Neville Moray, Department of Mechanical and Industrial Engineering, University of Illinois, 1206 West Green Street, Urbana, IL 61801

107. Dr. David Nelson, Director of Scientific Computing, ER-7, Applied Mathematical Sciences Office of Energy Research U. S. Department of Energy Washington, DC 20585

108. V. E. Oberacker, Department of Physics, Vanderbilt University, Box 1807, Station B, Nashville, TN 37235

109. J. T. Oden, Texas Institute for Computational Mechanics, University of Texas at Austin, Austin, Texas 78712

110. Joseph Oliger, Computer Science Department, Stanford University, Stanford, CA 94305

111. Robert O'Malley, Department of Mathematical Sciences, Rensselaer Polytechnic Institute, Troy, NY 12180-3590

112. James M. Ortega, Department of Applied Mathematics, Thornton Hall, University of Virginia, Charlottesville, VA 22901

113. Ron Peierls, Applied Mathematical Department, Brookhaven National Laboratory, Upton, NY 11973

114. Richard Pelz, Dept. of Mechanical and Aerospace Engineering, Rutgers University, Piscataway, NJ 08855-0909

115. Paul Pierce, Intel Scientific Computers, 15201 N.W. Greenbrier Parkway, Beaverton, OR 97006

116. Robert J. Plemmons, Departments of Mathematics and Computer Science, North Carolina State University, Raleigh, NC 27650

117. Jesse Poore, Computer Science Department, University of Tennessee, Knoxville, TN 37996-1300

118. Andrew Priestley, Institute for Computational Fluid Dynamics, Reading University, Reading RG6 2AX, ENGLAND

119. Lee Riedinger, Director, The Science Alliance Program, University of Tennessee, Knoxville, TN 37996

120. Patrick Roache, Ecodynamics Research Associates Inc., P.O. Box 8172, Albuquerque, New Mexico 87198

121. Garry Rodrigue, Numerical Mathematics Group, Lawrence Livermore National Laboratory, Livermore, CA 94550

122. Ahmed Sameh, Department of Computer Science, 200 Union Street, S.E., University of Minnesota, Minneapolis, MN 55455

123. Dave Schneider, University of Illinois at Urbana-Champaign, Center for Supercomputing Research and Development, 319E Talbot - 104 S. Wright Street Urbana, IL 61801

124. David S. Scott, Intel Scientific Computers, 15201 N.W. Greenbrier Parkway, Beaverton, OR 97006

125. Mark Shephard, Department of Civil Engineering, Mechanical Engineering and Rensselaer Design Research Center, Rensselaer Polytechnic Institute, Troy, New York 12180–3590

126. Dr. Bruce Simpson, Department of Computer Science, University of Waterloo, Waterloo, Ontario, Canada N2L 3G1

127. William C. Skamarock, 3973 Escuela Court, Boulder, CO 80301

128. Richard Smith, Los Alamos National Laboratory, Group T-3, Mail Stop B2316, Los Alamos, NM 87545

129. Peter Smolarkiewicz, National Center for Atmospheric Research, MMM Group, P. O. Box 3000, Boulder, CO 80307

130. Royce W. Soanes, Benet Laboratories, U.S. Army Armament Research, Development and Engineering Center, Close Combat Armaments Center, Watervliet, New York 12189

131. Stanly Steinberg, Department of Mathematical Statistics, University of New Mexico, Albuquerque, New Mexico, 87131

132. Jurgen Steppeler, DWD, Frankfurterstr 135, 6050 Offenbach, WEST GERMANY

133. Rick Stevens, Mathematics and Computer Science Division, Argonne National Laboratory, 9700 South Cass Avenue, Argonne, IL 60439

134. Paul N. Swarztrauber, National Center for Atmospheric Research, P. O. Box 3000, Boulder, CO 80307

135. Barna A. Szabo, Center for Computational Mechanics, Washington University, St. Louis, Missouri 63130

136. Wei Pai Tang, Department of Computer Science, University of Waterloo, Waterloo, Ontario, Canada N2L 3G1

137. Harold Trease, Los Alamos National Laboratory, Mail Stop B257, Los Alamos, NM 87545

138. Robert G. Voigt, National Science Foundation, Room 417, 1800 G Street N.W., Washington, DC, 20550

139. Mary F. Wheeler, Rice University, Department of Mathematical Sciences, P. O. Box 1892, Houston, TX 77251

140. Andrew B. White, Los Alamos National Laboratory, P. O. Box 1663, MS-265, Los Alamos, NM 87545

141. David L. Williamson, National Center for Atmospheric Research, P. O. Box 3000, Boulder, CO 80307

142. Samuel Yee, Air Force Geophysics Lab, Department LYP, Hancom AFB, Bedford, MA 01731

143. O. C. Zienkiewics, Institute for Numerical Methods in Engineering, University College of Swansea, Swansea, SA2 8PP, Wales, United Kingdom

144. Office of Assistant Manager for Energy Research and Development, U.S. Department of Energy, Oak Ridge Operations Office, P. O. Box 2001, Oak Ridge, TN 37831-8600

145–146. Office of Scientific & Technical Information, P. O. Box 62, Oak Ridge, TN 37831